1965

Neutron bombardment reduction of transistor current gain

Charles Alvin Goben
Iowa State University

NEUTRON BOMBARDMENT REDUCTION OF TRANSISTOR CURRENT GAIN

by

Charles Alvin Goben

A Dissertation Submitted to the
Graduate Faculty in Partial Fulfillment of
The Requirements for the Degree of
DOCTOR OF PHILOSOPHY

Major Subject: Electrical Engineering

Approved:

Signature was redacted for privacy.

In Charge of Major Work

Signature was redacted for privacy.

Head of Major Department

Signature was redacted for privacy.

Dean of Graduate College

Iowa State University
Of Science and Technology
Ames, Iowa

1965

TABLE OF CONTENTS

TABLE OF CONTENTS (Continued)

LIST OF ILLUSTRATIONS

LIST OF ILLUSTRATIONS (Continued)

I. INTRODUCTION

The decrease in transistor current gain observed upon exposure to neutron irradiation (1) has, in the past, been attributed primarily to the neutron-induced reduction in minority carrier lifetime in the base region, that is, to the resultant reduction of the base recombination term (2 - 6). Recent investigations (7, 8) have shown that the falloff of the transistor current gain at low currents in non-irradiated transistors is caused by a reduction in the emitter efficiency. This suggests the possibility that the emitter efficiency might also play an important role in transistor gain changes resulting from irradiation. To ascertain the role of the emitter efficiency, a more detailed study of the degradation of transistors in a radiation environment is required.

In the past several components of base current have been identified in non-irradiated transistors and these are tabulated in Figure 1. The first of these components is the bulk recombination-generation current which follows the ideal diffusion theory first given by Shockley (9) for uniform base transistors and later extended to the general case by Moll and Ross (10). It has a voltage dependence of $\exp(\frac{q}{kT}V)$. The second component is a recombination current in the transition (space charge) region. The voltage dependence of this second component approximates $\exp(\frac{q}{2kT}V)$ at low current densities (11). A third component has been identified as originating at the perimeter of the emitter (7, 8, 12), that is, where the emitter-base junction intersects the surface. Iwersen (7) suppressed this component by placing a guard ring on the emitter and applying a bias from emitter contact to guard ring. The voltage dependence of this particular component of current is as $\exp(\frac{q}{nkT}V)$, where n is approximately 1.5. A fourth component of current stems from surface channels and varies with voltage as $\exp(\frac{q}{mkT}V)$, where m is usually

CURRENT COMPONENT	VOLTAGE DEPENDENCE
BULK RECOMBINATION-GENERATION OR IDEAL DIFFUSION CURRENT	$\exp(qV/kT)$
BULK RECOMBINATION-GENERATION IN THE TRANSITION (SPACE-CHARGE) REGION	$\exp(qV/2kT)$
SURFACE RECOMBINATION-GENERATION CURRENT IN THE TRANSITION (SPACE-CHARGE) REGION	$\exp(qV/nkT)$ $n \approx 1.5$
SURFACE CHANNEL CURRENT	$\exp(qV/mkT)$ $2 \leq m \leq 4$

Figure 1. Current components associated with a p-n junction and their voltage dependence

between two and four for silicon junctions, although values larger than four have been noted for large channels (7, 11, 12).

As will be shown in the present work, neutron irradiation of p-n junction devices produces a component of current which varies as $\exp(\frac{q}{nkT}V)$, where n is approximately 1.5. This component of current is induced in the bulk transition region and dominates the transistor current gain over a wide range of current levels. These findings imply that the emitter efficiency plays a much more important role in radiation-induced changes in current gain than has been assumed in the past.

In 1949, Shockley (9) pointed out that the injected minority carrier current in the base of a transistor depended on the ratio of the minority carrier mobility to the base doping, i. e., the sheet carrier density (10). Shockley further pointed out that, in the absence of collector mutiplication, the collector current is just this injected minority carrier current modified by a recombination term, the base transport factor (base recombination term), to account for the carriers which recombine in the base region. The base current is composed of this recombination current, the space charge recombination current, and the surface recombination current. Shockley then derived an expression for the current gain which ignored these fundamentally different currents.

Ignoring these different components of current apparently led previous researchers in the field of radiation behavior of transistor current gain to erroneous conclusions.

From Shockley's work it may be seen that the best approach for studying the emitter efficiency in a p-n junction device is to ignore the simple expressions presented in the literature and study the components of current associated with the p-n junction. This may be accomplished by operating a transistor with a bias applied emitter-to-base and the collector shorted (to prevent the possibility of collector multiplication).

Operation in this manner leads to a collector current which is the ideal current component and a base current which contains all the non-ideal components of current originating in the transition region or on the semiconductor surfaces.

The above discussion also makes clear that a detailed study of these aspects can be most conveniently performed by examining the logarithm of collector and base current as a function of the emitter-to-base voltage. Since the various current components have a different voltage dependence, they can then be resolved and studied individually. Having understood the current components in terms of the emitter-to-base voltage, it is readily possible to translate the results into commonly used transistor parameters. This dissertation reports the results of such an investigation.

II. DISCUSSION OF PREVIOUS WORK

Much work has been done in the area of both permanent and transient radiation effects on semiconductors and semiconductor devices (1). A very small amount of this work has been in the area of examining the degradation of transistor current gain in detail (2 - 6) while most of the work has been in the area of characterizing the degradation of transistor gain and other easily measured transistor parameters at particular bias conditions (13 - 22), or in measuring the effects of radiation on bulk semiconductor materials (23 - 28).

Transient radiation effects in semiconductor materials and devices are associated with the creation of excess hole-electron pairs. Transient effects of radiation disappear after the exciting radiation is removed in times on the order of the minority carrier lifetime. Permanent damage is associated with damage to the lattice whether or not it anneals out with time and temperature. Sander has recently shown (22) that significant annealing occurs at room temperature and that this annealing is completed in times of the order of tens of seconds after the irradiation is stopped. The remaining damage is stable at room temperature with less than a three percent change in 3000 hours (29). The permanent damage with which this dissertation is concerned is the room-temperature-stable permanent damage.

Crystal lattice defects introduced by irradiation act as recombination sites and hence decrease the minority carrier lifetime. Crystal lattice defects, through impurity scattering and compensation of shallow impurities, reduce the carrier mobilities and the carrier concentration. Fast-neutron irradiation is particularly effective in damaging crystal lattices in that thousands of atoms may be removed from their lattice sites as the result of a single collision (26).

Loferski (2) in the first treatment, 1958, of transistor current gain degradation examined the simple expression (30 - 35) for emitter efficiency involving only the ratios of the sheet resistivities of the base and emitter regions (36, 37) and concluded that the emitter efficiency should increase with neutron bombardment but that the change would be negligible. Using a linear dependence of the reciprocal lifetime on neutron flux, Loferski modified Webster's equation (31) for dependence on neutron flux and concluded that the reciprocal of the common-emitter current gain should vary linearly with flux. Discrepancies between theory and experiment were attributed to experimental error and the use of incorrect values for the constants in his theoretical expression.

Messenger and Spratt (3) in their analysis, 1958, of transistor gain degradation due to neutron bombardment, again assumed the emitter efficiency to be essentially independent of flux. The theoretical analysis consisted of applying Shockley-Read (38, 39) statistics to Webster's equation. From this analysis, Messenger and Spratt were able to calculate the energy of an assumed single level for the recombination sites. The recombination sites were assumed to be in the bulk base region and to act only through lifetime degradation. Cross-sections for interaction with the mobile carriers were also calculated. Discrepancies between theoretical and experimental results were attributed to lack of precise knowledge of the lifetime damage constant and experimental error.

Easley and Dooley (4) in their analysis, 1960, assumed the emitter efficiency to be independent of neutron flux and further that the emitter efficiency and collector multiplication factor were equal to unity. Thus, the common-base current gain reflected only the base transport factor (base recombination term). The expression (30 - 35) for the base recombination term was modified to exhibit a dependence on neutron flux by assuming a flux dependent lifetime and an electrical base width that varied with

irradiation due to changes in the carrier concentration. The expression which Easley and Dooley derived simplified to a linear dependence on flux for the assumption of fluxes too low to cause appreciable carrier removal. Experiments were carried out in a steady state reactor, with measurements made in-core, in an attempt to verify the theory. Disagreements were attributed to partial annealing of the radiation damage during bombardment.

Hood, in a recent analysis (5), 1964, of neutron degradation of transistor current gain, allowed the emitter efficiency to vary with neutron flux through the inclusion of the back-injection term and a simplified form of the Sah-Noyce-Shockley (11) expression for the normal bulk space charge recombination-generation term. The back injection into the emitter is normally negligible because of the high doping in the emitter and the normal bulk space charge is negligible at emitter-base biases greater than 0.3 volts as may be seen from the curves in section III. The discrepancy between Hood's theoretical and experimental results were greatest at low current levels where it would be expected to be the least. This discrepency was attributed to neglecting the collector leakage current in his analysis.

It is interesting to consider why the reciprocal common-emitter current gain should vary linearly with integrated neutron flux (ϕ) at low flux levels. For reasonably low levels of flux, the simplified form of the expression derived by Easley (4) for the base transport factor (β) should hold, and may be written as

$$\frac{\beta}{\beta_o} = 1 - k_1 \cdot \phi. \qquad (1)$$

From section III the emitter efficiency (γ) at a particular bias and at low flux levels may be written as

$$\frac{\gamma}{\gamma_o} = \frac{1}{1 + k_2 \cdot \phi} \cdot \tag{2}$$

The reciprocal of the common emitter current gain (h_{FE}) may be written in terms of the base transport factor (base recombination term) and emitter eficiency as

$$\frac{1}{h_{FE}} = \frac{1}{\alpha} - 1$$

$$= \frac{1}{\gamma\beta} - 1. \tag{3}$$

The collector multiplication factor has been assumed to be unity. Substituting equations 1 and 2 into equation 3 one obtains

$$\frac{1}{h_{FE}} = \frac{1}{\gamma_o \beta_o} \cdot \frac{1 + k_2 \cdot \phi}{1 - k_1 \cdot \phi} - 1. \tag{4}$$

Expanding equation 4 and keeping only the first order terms, one obtains a linear dependence of the reciprocal common emitter current gain on flux.

$$\frac{1}{h_{FE}} = \left(\frac{1}{\gamma_o \beta_o} - 1\right) + (k_1 + k_2) \cdot \phi$$

$$= \frac{1}{h_{FEo}} + k_3 \cdot \phi. \tag{5}$$

At higher levels of flux, about 10^{14} neutrons/cm^2 for 2N914 transistors, the higher order terms cannot be discarded and, in addition, the exact expressions for base recombination term and emitter efficiency must be used in place of equations 1 and 2.

III. EXPERIMENTAL AND THEORETICAL INVESTIGATION

A. Experimental Approach

A number of experiments were designed to study, in greater detail, the role of the emitter efficiency in neutron bombarded transistors.

The first set of these experiments consisted of the measurement of the current-voltage characteristics with integrated neutron flux as a parameter. From these data the conclusions were drawn:

1 - that neutron bombardment introduced a component of base current,

2 - this neutron-induced base current component depended on junction voltage as $\exp(\frac{q}{nkT}V)$, $n \approx 1.5$,

3 - this neutron-induced component was of bulk origin rather than surface origin as might have been concluded from its voltage dependence,

4 - the effect of this neutron-induced component of base current was the degradation of the emitter efficiency.

The second set of these experiments consisted of designing and fabricating special test structures to allow the measurement of base region parameters so that the base recombination term could be extracted from the data. From data measured on these special test structures, the following conclusions were drawn:

1 - degradation of base region parameters with neutron bombardment is similar to the degradation of parameters in bulk material,

2 - the base recombination term degraded with neutron bombardment, but not as substantially as had been supposed in the past.

The third set of experiments was concerned with verifying mathematical derivations predicting the behavior of the various base current components under transverse bias with measurements performed on the test structures.

The fourth set of experiments was designed to verify that the observed effects of neutron bombardment on the devices used for this study (the special test structures) were general phenomena observable in any transistor structure.

Additional experiments were designed and performed to study the effects of temperature and annealing upon the neutron-induced component of current. From these data, the conclusion was drawn that the annealing of damage sites in neutral and space charge regions of the semiconductor apparently differed.

Experiments were designed and performed (with electron irradiation) to substantiate a possible explanation of the origin of the neutron-induced component of current.

B. Single-Base Transistors

Experimental techniques used in examining the characteristics of p-n junction devices in terms of the various components of current are shown in Figure 2. The transistor is operated with both base and collector grounded and a bias voltage is applied emitter-to-base. The type of transistor chosen for this study is an NPN silicon planar epitaxial transistor with the ring-dot structure illustrated in the upper left corner of the figure. The curve shown was selected as being typical of a large number of devices measured. Note that a line of reciprocal slope of kT/q fits the collector current precisely over 8 decades of current. The voltage deviation or "bendaway" of the collector current from the ideal line at high currents is caused by the transverse voltage drop in the base

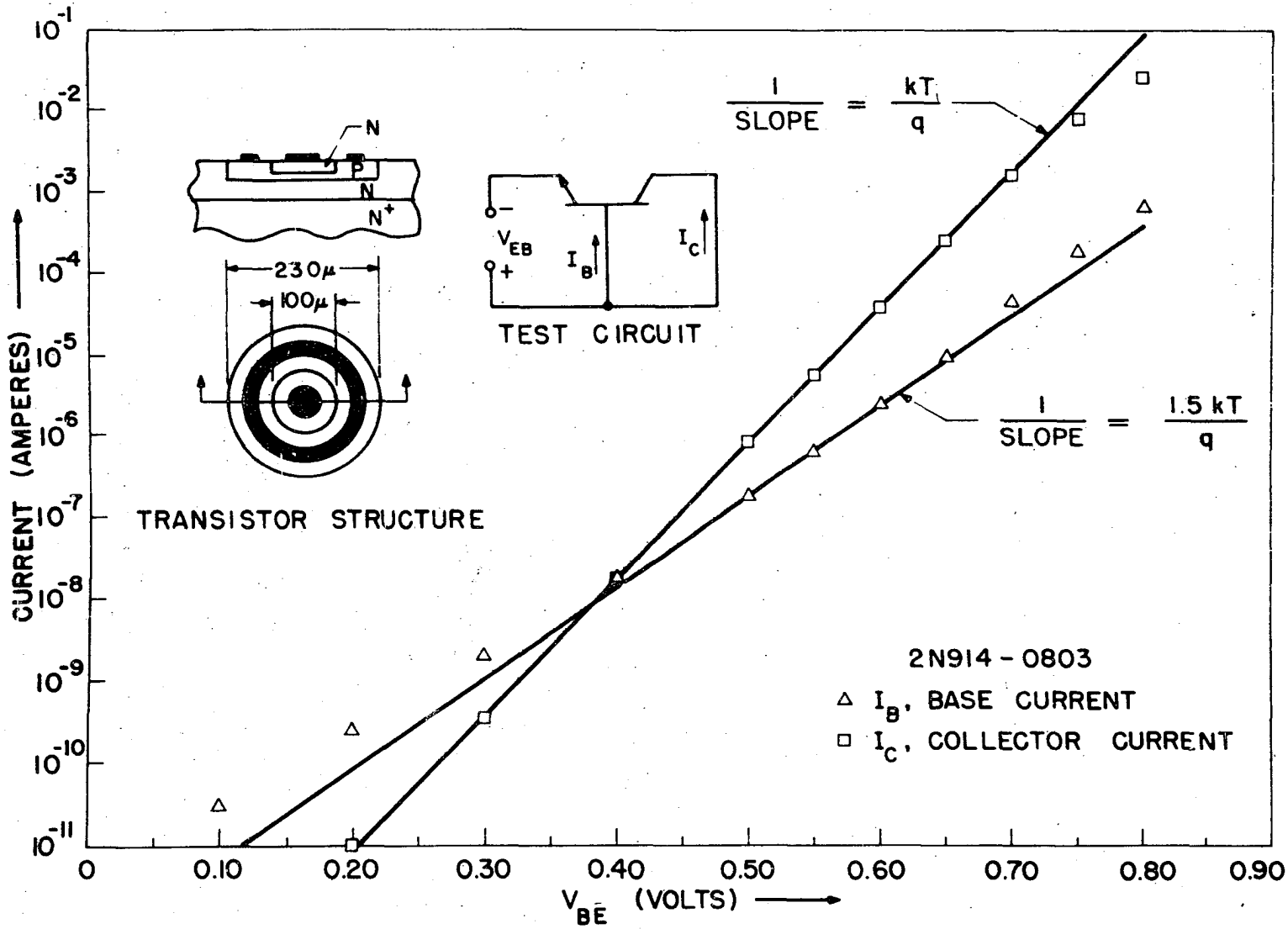

Figure 2. Circuit diagram and current-voltage characteristics

region under the emitter as a result of the fringing or crowding of the injected emitter current which is the direct result of the transverse voltage drop. The linearity of the collector current curve implies that the base recombination term is independent of current density. Note that a line of reciprocal slope of 1.5kT/q has been fitted to the center portion of the base current data. At higher current levels, the base current data rise toward a reciprocal slope of kT/q, then bend away, as does the collector current. At lower current values, the base current tends to a reciprocal slope approaching 2kT/q.

Since never more than two components are significant at any bias voltage and there is a wide range over which only one component is significant, it is possible to resolve the base current into separate components, as illustrated in Figure 3. First, the "n = 1.5 component" of current is extrapolated to both higher and lower currents and subtracted from the measured values of base current. At the upper end of the curve, this results in a component of base current which follows, within experimental error, the collector current, indicating that this is indeed an ideal component of current. By correcting this current component by the voltage deviation of the collector current from the extrapolated ideal line, the corrected base-current component can be obtained that would flow if the base-region resistance were negligibly small. This technique yields corrected data points that fit a straight line of a reciprocal slope of kT/q. Similarly, at the lower current values, subtracting the extrapolated "1.5 component" of current from the measured base-current data yields points through which the line of reciprocal slope 2kT/q may be drawn.

When these transistors are bombarded with high-energy neutrons to a total integrated flux of 2×10^{14} neutrons/cm^2 (with neutron energy greater than 0.01 MeV), curves as shown in Figure 4 are obtained. Note that the common-emitter DC current gain (ratio of collector current to

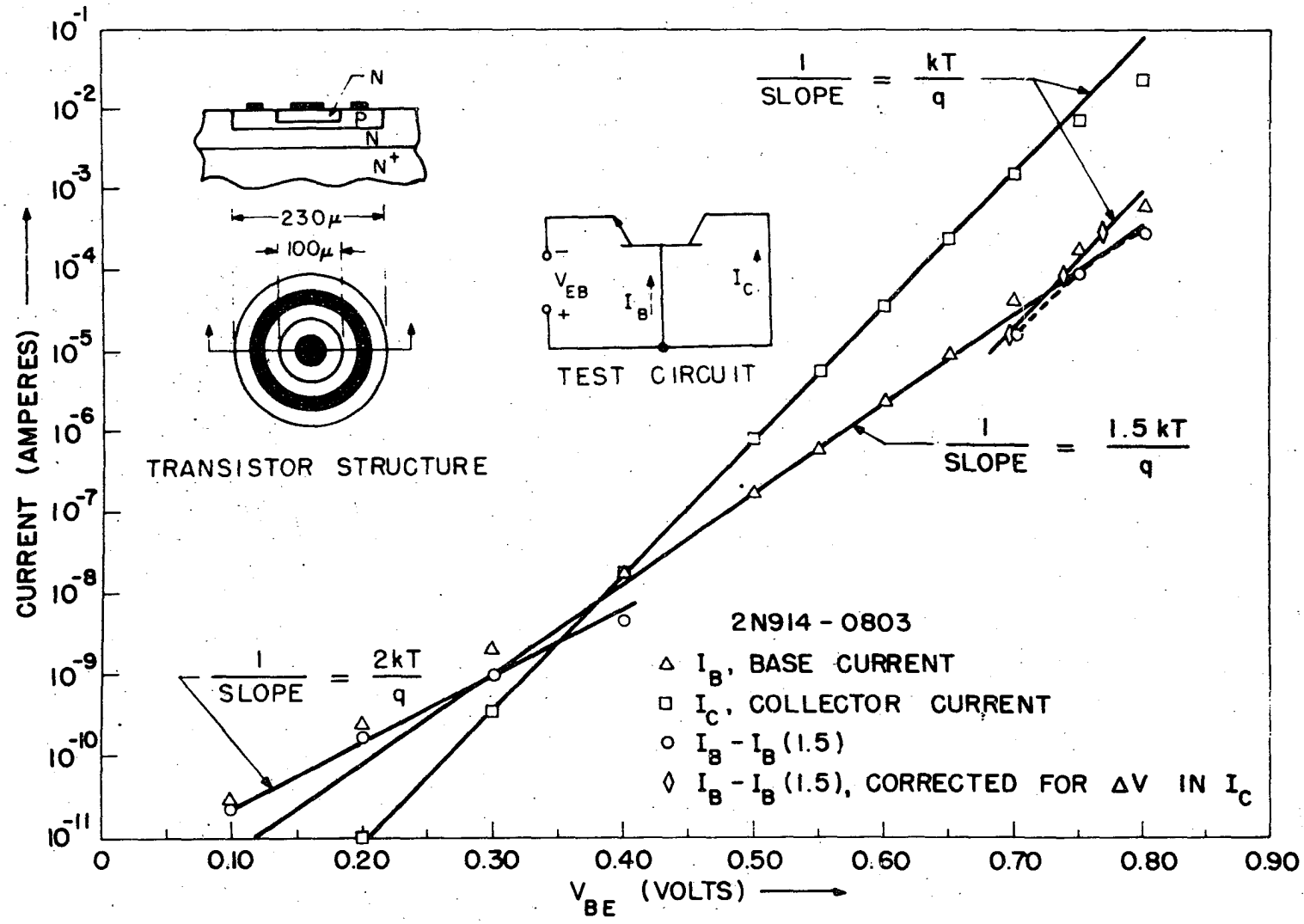

Figure 3. Current components and their resolution

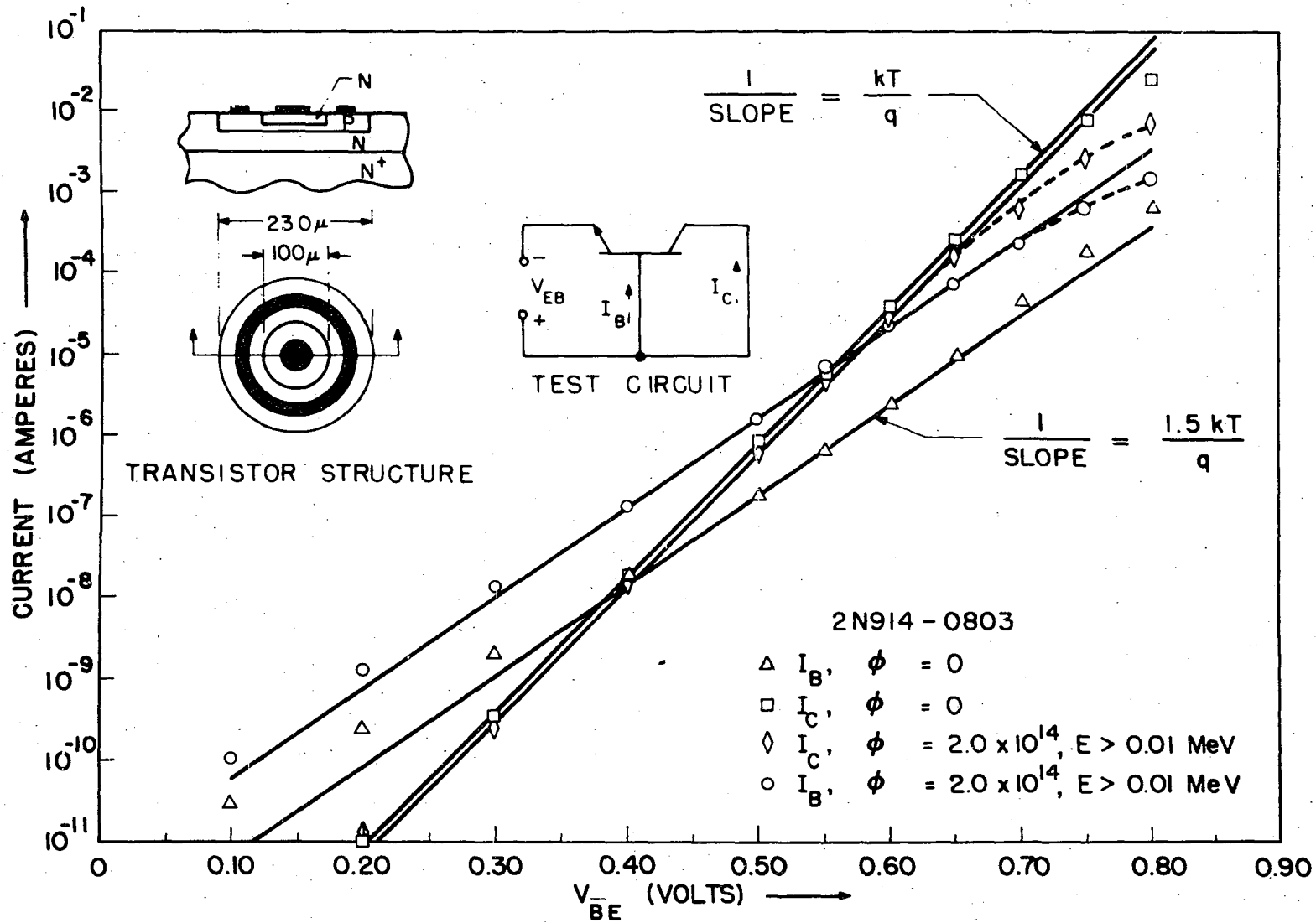

Figure 4. Pre- and post-irradiation I-V characteristics

base current), which, on this semilogarithmic plot, is simply the distance between the collector current and base current, has decreased substantially. Note also that the collector current still fits the straight line with the reciprocal slope of kT/q for many decades, implying that the base recombination term in these transistors is still independent of current density. The slight decrease in the collector current is attributable primarily to a decrease in the base recombination term. The voltage "bendaway" at high collector currents sets in somewhat earlier because of the combination of a slight increase in sheet resistance in the base region under the emitter and larger base currents flowing through this resistance. The base current has increased by a factor of 8.5 and a line of reciprocal slope of 1.5kT/q now fits the base current data over a much larger current range than in the preirradiated condition. In the unirradiated transistor, the component of current with a slope of approximately 1.5kT/q has been identified as a perimeter current as indicated earlier (7, 8, 11, 12). Hence, this "surface-perimeter component" of current would flow only in the highly doped and, hence, small resistance regions of the base surrounding the emitter. This resistance can be measured by biasing the emitter junction into breakdown and observing the differential resistance above breakdown. Since, in such planar structures, breakdown occurs at the perimeter, the slope will give the external base resistance, provided the current levels are kept low enough to prevent conductivity modulation. This has been done on a group of 10 transistors similar to the group irradiated. The average value of resistance for this current path was found to be 12.8 ohms and had a standard deviation of 1.5 ohms. This value differs sharply from the values of base-spreading resistance of 100 to 150 ohms for the current path of the component of base current which is flowing through the high-resistance base region under the emitter. The early onset of voltage "bendaway" of the collector current and the "bendaway" of the base current under the 1.5kT/q line

show that the neutron-induced "1.5 component" of current flows through a high resistance and cannot be attributed to a current of perimeter origin, but now must be attributed to a bulk recombination-generation current in the emitter-base transition (space charge) region.

Figure 5 displays, in an expanded scale, a portion of the base current versus emitter-base voltage data. From these data one finds that, at any constant voltage, the "1.5 component" of current is increasing proportional to flux. Thus, the analytical relation between the increase in base current and integrated neutron flux, ϕ, is given by

$$I_{B_{inc}} = K_1 \cdot A_E \cdot \phi \cdot \exp\left(\frac{q}{nkT}V\right), \qquad (6)$$

where n is approximately 1.5, A_E is the emitter area, ϕ is the integrated neutron flux, V is the emitter-to-base voltage, and the constant K_1 is 3.33×10^{-22} (amperes/cm^2)/(neutrons/cm^2). A volume dependence, rather than an area dependence, for the current increase due to the recombination term might have been expected. It should be appreciated, however, that as the bias on the emitter-base junction is increased from 0.1 volt to 1.0 volt, the depletion-layer width, and hence the volume, changes by only a factor of 3; the term $\exp(\frac{q}{nkT}V)$ changes by about 30,000,000. Additionally, one might expect the recombination statistics to vary through the depletion region, thus causing even less dependence on width and, therefore, on volume.

Figure 6 shows a small region of the collector-current data in an expanded scale. It can be seen that the collector current decreases with flux. This decrease in collector current must primarily be attributed to a decrease in the base recombination term for which the analysis of Easley (4, 6) should hold. For a closer analysis of this decrease, other variables influencing the collector current need to be considered. If

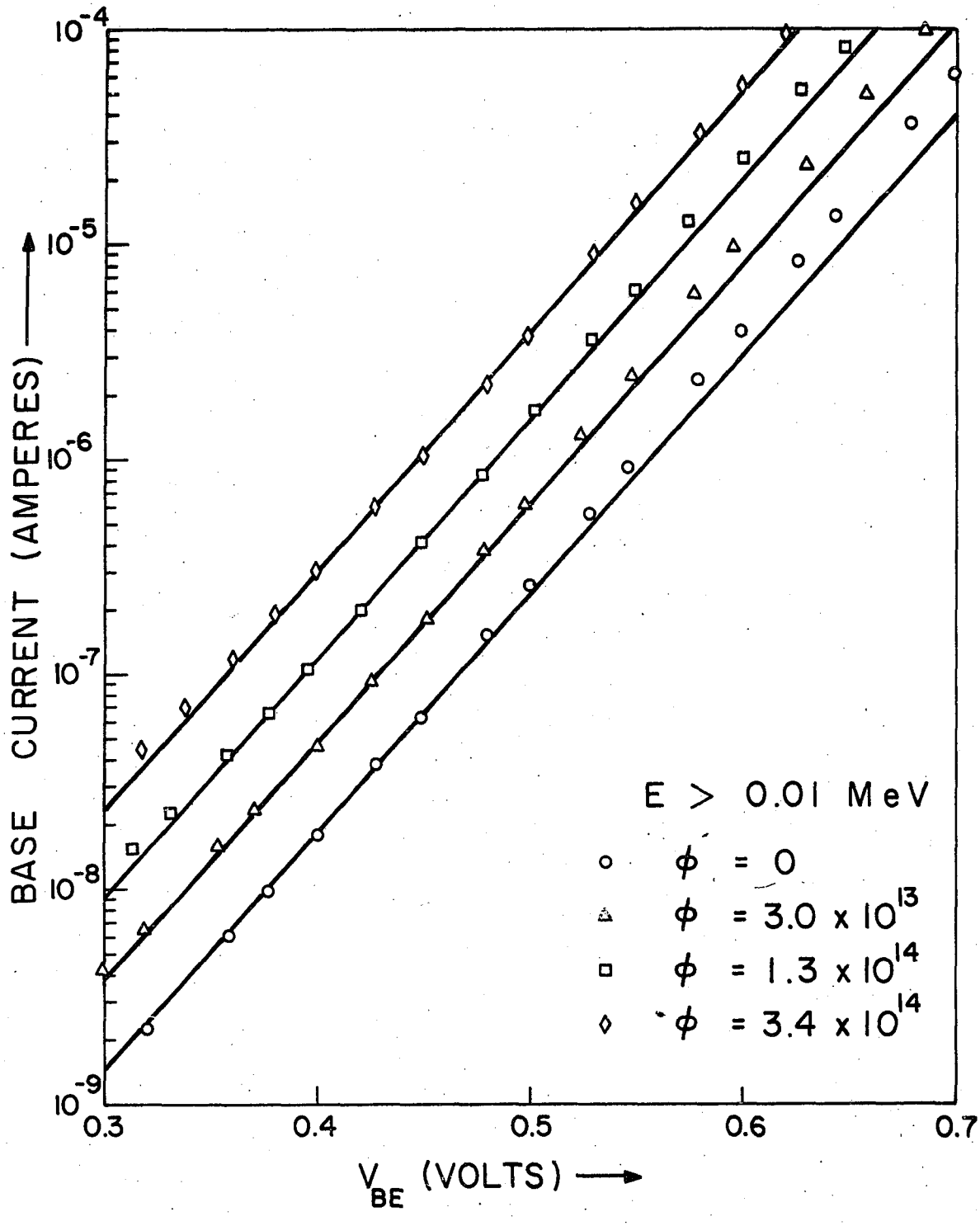

Figure 5. I_B vs V_{BE} with ϕ as parameter

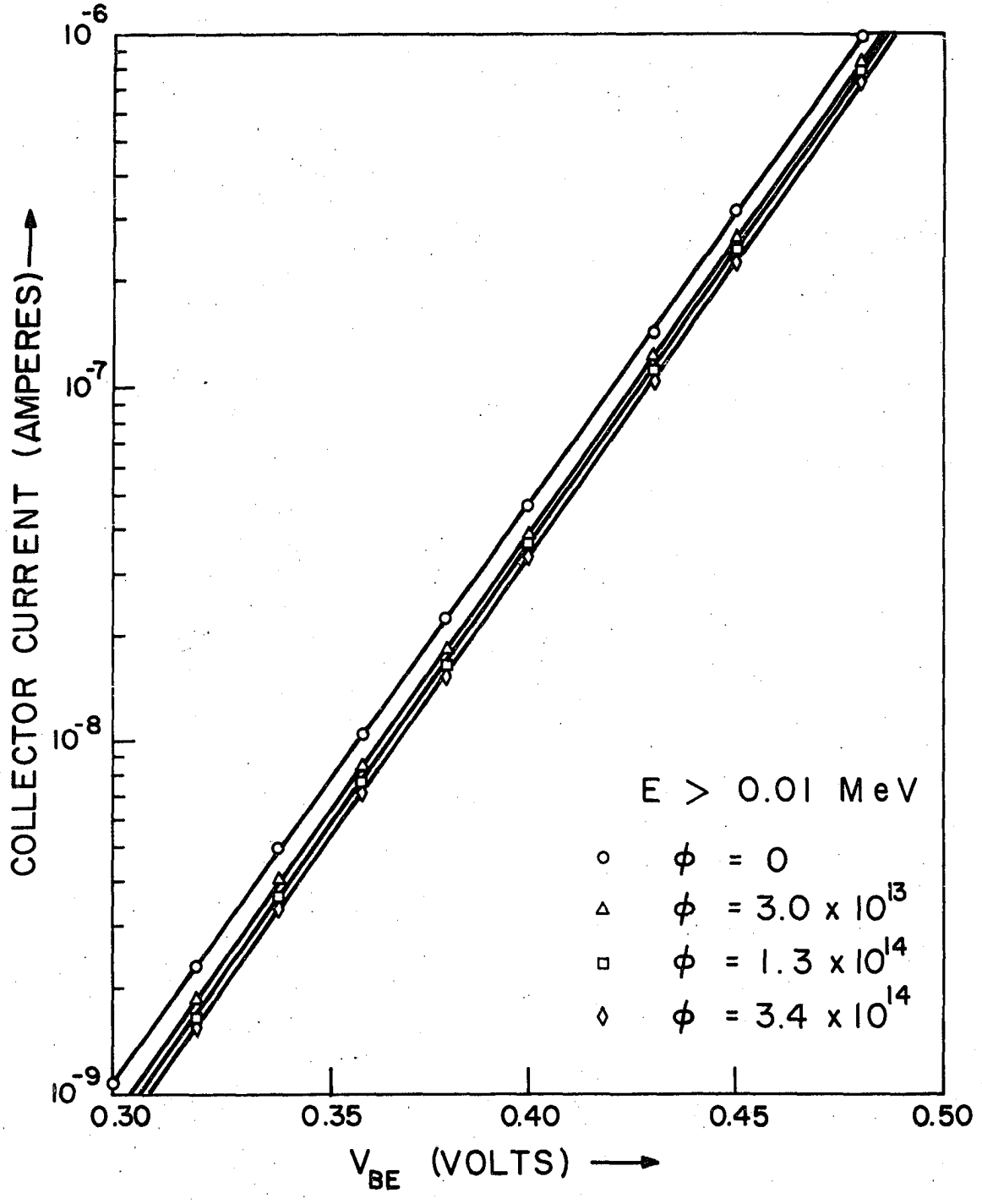

Figure 6. I_C vs V_{BE} with ϕ as parameter

recombination in the base can be neglected, the collector current, in terms of the emitter-to-base voltage, is given by the equation below (10):

$$I_C = \left(A_E \cdot n_i^2 \cdot kT \cdot \mu_n / \tilde{N}_A\right) \exp\left(\frac{q}{kT} V\right), \tag{7}$$

which is valid for the ratio of the diffusion length to base width large with respect to unity. In equation 7, n_i is the intrinsic carrier density, μ_n is the electron mobility in the base and $\tilde{N}_A$ is the number of majority carriers per unit area of the base region. To include recombination in the base, the collector current must be multiplied by the base recombination term, β. Of these variables, μ_n, $\tilde{N}_A$, and β will change with irradiation. To find changes in β from the changes in collector current, a knowledge of changes in μ_n and $\tilde{N}_A$ is required.

C. Test Structures

Test structures were designed to allow the measurement of the current-voltage characteristics, the sheet resistance in the base region, the Hall mobility, and the number of majority carriers per unit area in the base region.

The first structure illustrated in Figure 7 is simply the 2N914 silicon planar epitaxial transistor used in the measurements discussed. The second structure is a double-base transistor with the base leads brought out separately, making it a four-terminal device. This allows measurement of the sheet resistance in the base region under the emitter and allows biasing from one base contact to the other to change the distribution of current flow under the emitter ring. The third structure is essentially a van der Pauw (40 - 56) sample to allow the measurement of the Hall effect and sheet resistance in the base region. All test structures have impurity profiles and base, collector, and emitter dimensions identical to those commonly used in 2N914 transistors. All devices were

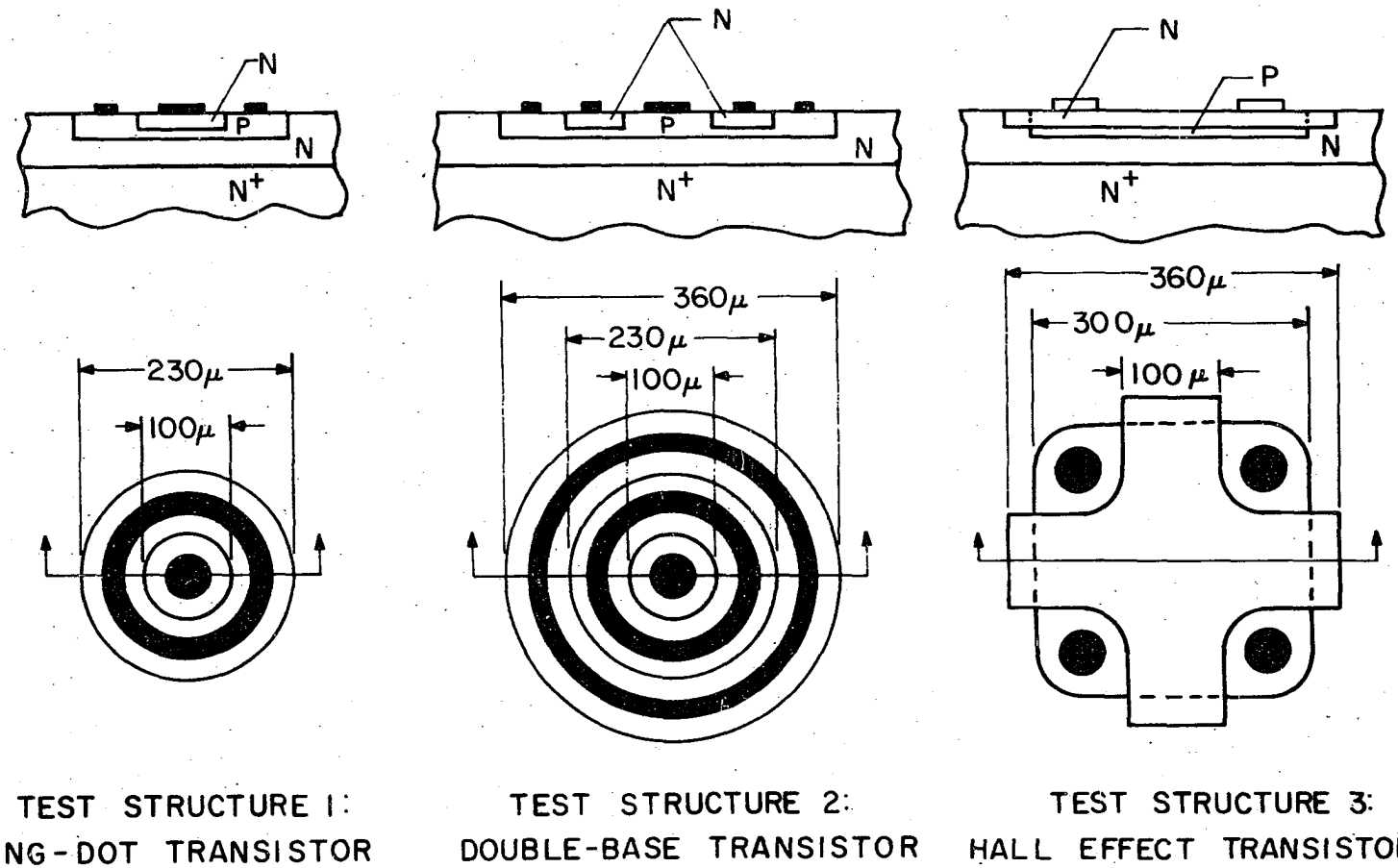

TEST STRUCTURE 1: RING-DOT TRANSISTOR

TEST STRUCTURE 2: DOUBLE-BASE TRANSISTOR

TEST STRUCTURE 3: HALL EFFECT TRANSISTOR

Figure 7. Test structures to correlate base region parameters with current-voltage characteristics

fabricated in the same diffusion run and the devices fabricated from a given slice of silicon were identified as such.

D. Test Equipments - General

Figure 8 shows the electronic data recording system I and the peripheral equipment. This is the recording system which was used to record most of the data taken in this series of experiments.

The sample is placed in the sample holder shown at the top of the figure. The John Fluke 383B supplies the base-emitter voltage via a path through the current sampler to the sample. Signals proportional to the sample current and voltage are routed from the sample holder back to the current sampler. A signal proportional to either the collector or the base current, whichever is being measured (only one current is measured at a time), appears at terminal J13 of the current sampler. This signal is then amplified by an amplifier, whose gain may be set to various values between 10 and 1000, and is then measured by one of the NLS M24 digital voltmeters in the data recording system. The voltage signal of the emitter-base voltage appears at terminal J2 of the John Fluke 383B voltage/current calibrator and is fed via a loop through the current sampler (J14-J12) to an NLS M24 digital voltmeter. The John Fluke 383B voltage/current calibrator is programmed for the specific emitter-base voltage desired for the particular base or collector current measurement by means of an automatic driver/programmer. The driver/programmer is fed via a loop through the current sampler (J8-J10) from the Dymec 2901A/2902A scanners in the data acquisition system. The data acquisition system itself is shown within the dashed lines in Figure 8. The two NLS model M24 digital voltmeters transmit signals to the Gulton Industries decoder. These signals consist of a 10-line code for each of the four digits, the polarity and the exponent of the reading. In addition there is a signal signifying end of count or end of sampling period from

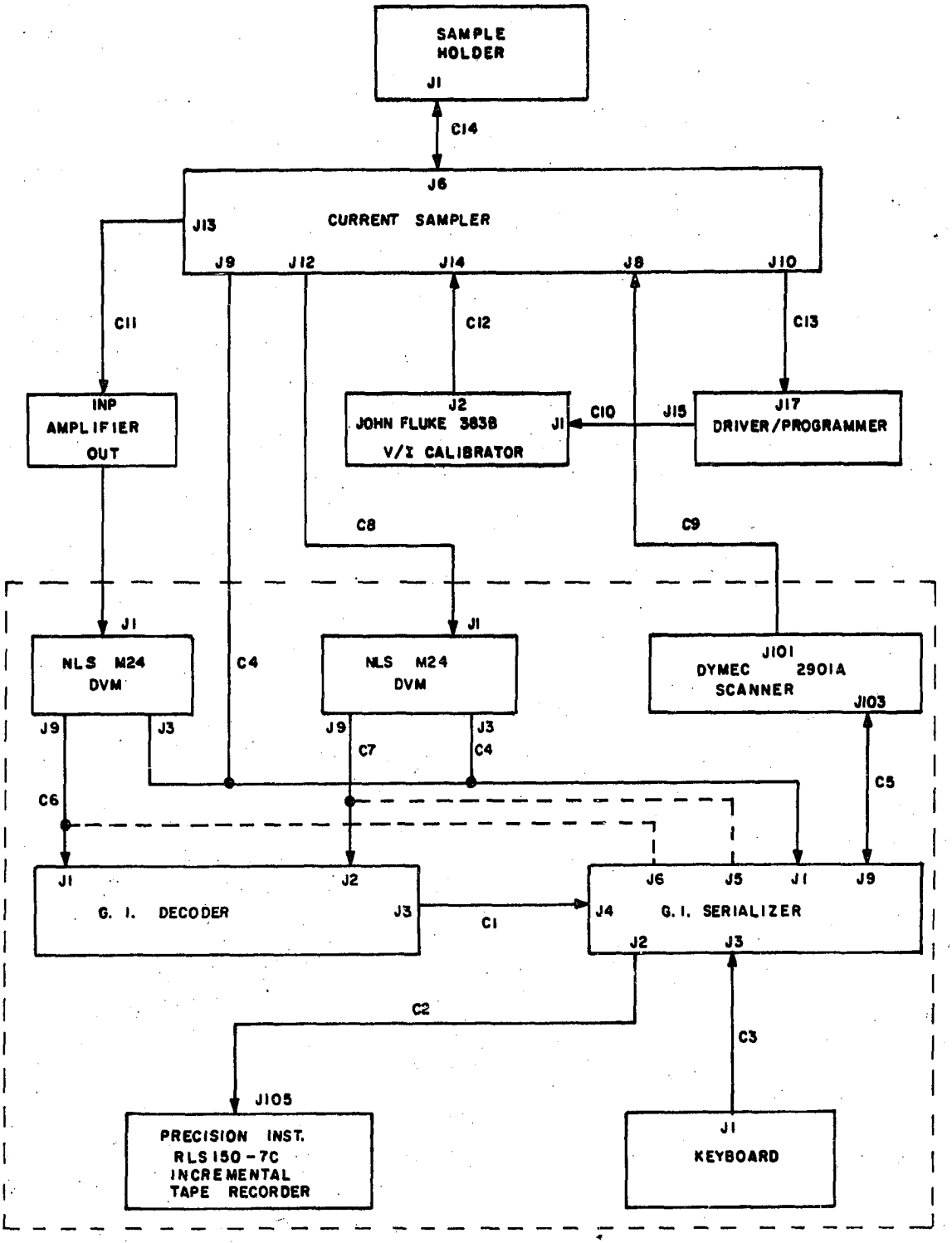

Figure 8. Block diagram of electronic data recording system I and peripheral equipment

each voltmeter. These signals are used by the Gulton Industries decoder by means of an AND circuit to tell the decoder that it is ready to decode the 10-line codes into 4-line codes. These 4-line codes are then passed to the Gulton Industries serializer where, in conjunction with a character (→) signifying beginning of data word, the two voltmeter readings are serialized. When serializing is completed, a command signal is given to the Precision Instruments model RSL150-7C Incremental Tape Recorder to accept the coded data word. The Invac keyboard provides a means of inserting manual or lead information at the beginning of the record for a particular data run.

A somewhat simpler data acquisition system (or data recording system) was built while awaiting completion of data acquisition system I and is shown in Figure 9. This data acquisition system used the same peripheral equipment as in the first data system. The second data system consisted of two Dymec 2401A digital voltmeters, two Dymec H25-562AR digital recorders, the Dymec 2901A master scanner/programmer and three Dymec 2902A slave scanner/programmers. This system prints out the data via the digital recorder onto a spool of paper which must be then taken to the keypunch office and punched onto cards. The data are then transferred to magnetic tape to be used by the computer data reduction program. This method, while somewhat slow and tedious, was the basis of a very workable system while the primary system was not operational.

The above two data acquisition systems with peripheral equipment are accurate for making measurements in the range of 10^{-11} amperes up to one ampere. For measurements of current at levels below 10^{-11} amperes, that is, for emitter-base voltages of less than 0.2 of a volt, it was necessary to take the data manually by means of the voltage supply and two Hewlett-Packard 425 microvolt-ammeters. The transistor in

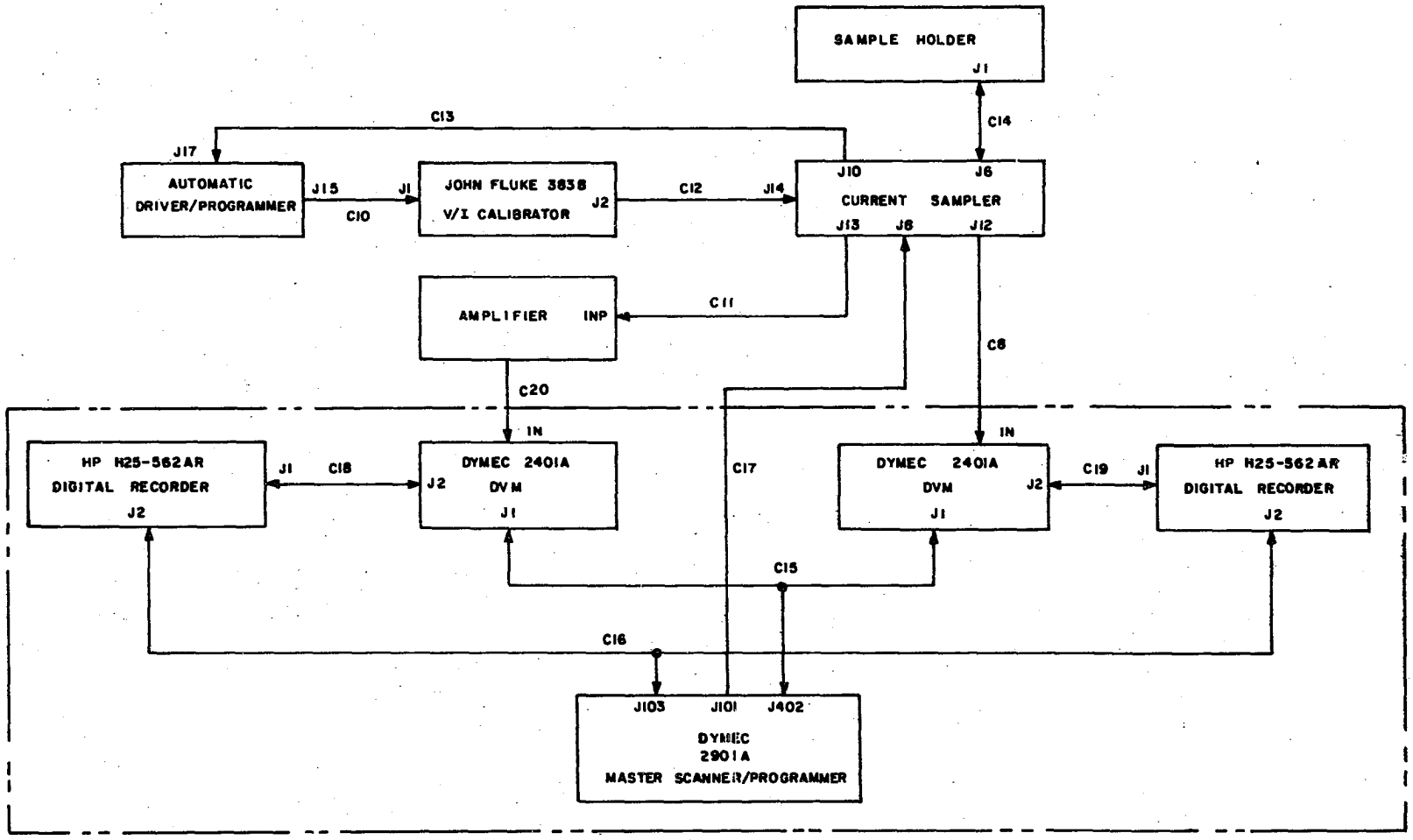

Figure 9. Block diagram of electronic data recording System II and peripheral equipment

this case was mounted in a special socket fabricated from the tee of a 50 ohm coaxial cable connection with 50 ohm cables used for connections to the voltage supply and to the two ammeters. It was necessary, in this low-level situation, to record the data manually and have it punched onto cards and translated to magnetic tape for use by the data reduction program.

E. Analysis of the Deviation of the Current-Voltage Characteristics From the Ideal Situation for a Ring-Dot Structure

As pointed out previously, the collector current of a normal transistor is observed to follow an $\exp(\frac{q}{kT} V_{BE})$ dependence over 8 to 9 decades of current, and, then, to bend away or deviate from this ideal dependence at high current levels. This "bendaway" or deviation was observed to be caused by fringing (crowding) of the injected emitter current due to the transverse voltage drop in the base region under the emitter which, in turn, is caused by the base current flowing in the base region under the emitter out to the base contact.

As was noted from observation of the collector- and base-current characteristics as a function of applied base-emitter voltage, there are three components of base current in a normal transistor. The first of these components varies with voltage as $\exp(\frac{q}{2kT} V)$ and has been explained by Sah, Noyce, and Shockley (11) as the bulk space-charge recombination-generation current. This component is negligible compared to the other components above 0.3 volt. Hence, it does not contribute to the deviation of the collector current from the ideal voltage dependence. The second component of base current is the bulk diffusion current or ideal bulk recombination-generation current which varies with voltage as $\exp(\frac{q}{kT} V)$ and does contribute to the deviation of the transistor

current-voltage characteristics from the ideal. The third component of base current varies with applied bias as $\exp(\frac{q}{nkT}V)$, where $n \approx 1.5$. If this component of current is of surface-perimeter origin, as is apparently the case for unirradiated transistors, it cannot contribute to the transverse biasing effect as does the ideal component of base current and, hence, cannot cause any deviation of the current-voltage characteristics from the ideal. It is observed, however, that an "n = 1.5 component" of base current is induced upon neutron irradiation which is proportional to neutron flux and originates in the bulk space-charge region. This neutron-induced component can contribute to the transverse biasing effect and, hence, the deviation of the current-voltage characteristics from the ideal.

It is instructive to examine mathematically the dependence of the current-voltage deviation on the base-current components. The equations governing this relationship may be formulated as follows.

The transverse differential voltage drop at any radius r (see Figure 10) is

$$dV(r) = I(r)\left(\frac{dR(r)}{dr}\right)dr, \tag{8}$$

where $(dR(r)/dr)$ is the radial derivative of the resistance and, for a ring-dot structure, is given by

$$\left(\frac{dR(r)}{dr}\right) = \frac{\rho_s}{2\pi r}. \tag{9}$$

In equations 8 and 9, ρ_s is the sheet resistivity in the base region under the emitter and I(r) is the current flowing at radius r, which is given by

$$I(r) = I_n(r) + I_i(r), \tag{10}$$

where $I_n(r)$ and $I_i(r)$ refer to the "n = 1.5" and ideal (n = 1) components of base current. Their dependence on voltage is given by

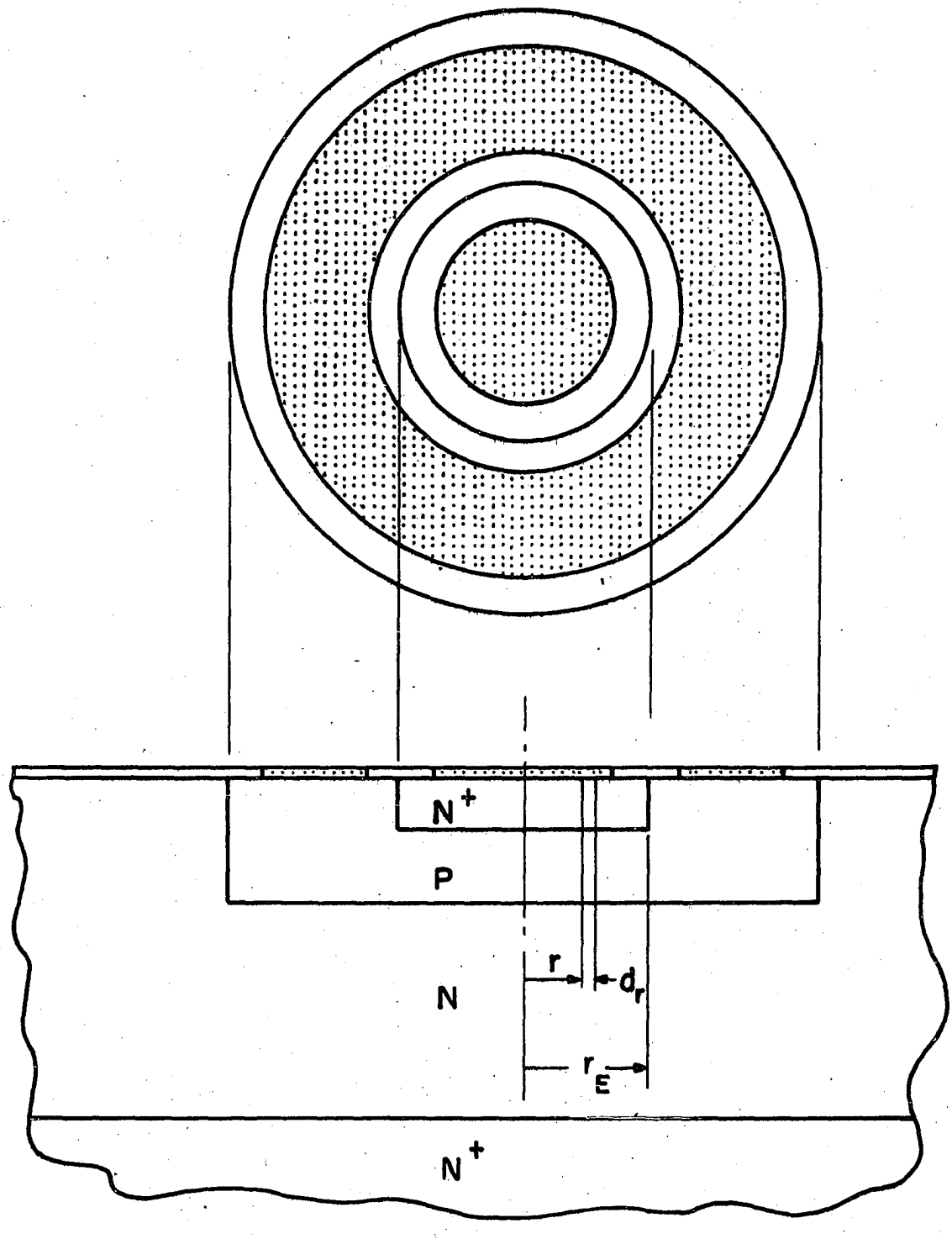

Figure 10. Geometry of ring-dot transistor structure

$$dI_n(r) = J_{noo} \exp\left(\frac{q}{nkT}\left[V_o + V(r)\right]\right) 2\pi r\,dr$$

$$dI_i(r) = J_{ioo} \exp\left(\frac{q}{kT}\left[V_o + V(r)\right]\right) 2\pi r\,dr. \tag{11}$$

In equation 11 J_{noo} and J_{ioo} are the low level current densities of the two components and V_o is the voltage drop across the emitter-base junction at the center of the emitter. The potential, V_o, may be accounted for by defining

$$J_{no} = J_{noo} \exp\left(\frac{q}{nkT} V_o\right)$$

$$J_{io} = J_{ioo} \exp\left(\frac{q}{kT} V_o\right). \tag{12}$$

Substituting equation 9 into equation 8 and differentiating with respect to the radius, one obtains

$$V''(r) = I'(r) \frac{\rho_s}{2\pi r} + \left(\frac{-1}{r}\right) I(r) \frac{\rho_s}{2\pi r} \tag{13}$$

Substituting equations 8, 9, 11, and 12 into equation 13 and rearranging, one obtains a differential equation for the voltage.

$$V''(r) + \frac{1}{r} V'(r) - \rho_s\left(J_{io} \exp\left[\frac{q}{kT} V(r)\right] + J_{no} \exp\left[\frac{q}{nkT} V(r)\right]\right) = 0 \tag{14}$$

Equation 14 is intractable and must be solved by numerical methods.

There are two cases of interest which can be solved in closed form:

Case 1 -- The ideal component of current is responsible for all the transverse voltage drop. This corresponds to the prebombardment situation.

Case 2 -- The "n = 1,5 component" of current induced by neutron irradiation is of such magnitude as to dominate the transverse voltage drop. This corresponds to the situation existing after exposure of the devices to a total integrated flux of a few times 10^{14} neutrons/cm^2.

The equation

$$V''(r) + \frac{1}{r}V'(r) - K \exp(cV(r)) = 0, \tag{15}$$

with initial conditions $V'(0) = V(0) = 0$, has the solution (57)

$$\exp(cV(r)) = \frac{1}{\left(1 - \frac{cK}{8}r^2\right)^2} . \tag{16}$$

Case 1 has been examined by Looney (58) using a slightly different technique than will be employed here. Case 2 may be generalized to include Case 1 as a special situation by not defining the value of n until the analysis is completed. In equation 16, letting c equal $\frac{q}{nkT}$ and K equal $\rho_s J_{no}$, one obtains

$$\exp\left(\frac{q}{nkT}V(r)\right) = \frac{1}{\left(1 - \frac{q}{nkT} \cdot \frac{\rho_s J_{no}}{8} \cdot r^2\right)^2} . \tag{17}$$

The total base current in this case is

$$I_n = \int_0^{r_E} J_{no} \exp\left(\frac{q}{nkT}V(r)\right) 2\pi r dr$$

$$= \pi J_{no} \int_0^{r_E} \frac{d(r^2)}{\left(1 - \frac{q}{nkT} \cdot \frac{\rho_s J_n}{8} \cdot r^2\right)^2}$$

$$= \pi J_{no} \int_0^{r_E^2} \frac{dy}{\left(1 - \frac{q}{nkT} \frac{\rho_s J_{no}}{8} y\right)^2}$$

$$= \frac{8\pi nkT}{q\rho_s} \left[\frac{1}{1 - \frac{q\rho_s J_{no}}{8nkT} r_E^2} - 1 \right] \tag{18}$$

Equation 18 may be solved for J_{no} in terms of I_n. The result is

$$J_{no} = \frac{8\pi nkT}{q\rho_s \pi r_E^2} \left[\frac{1}{1 + \frac{q\rho_s}{8\pi nkT} I_n} - 1 \right]. \tag{19}$$

The surface-perimeter current, I_{s-p}, must be subtracted from the total base current, I_B, to obtain I_n if the surface-perimeter current is not small.

It is possible to define a voltage, V_{un}, which, if applied uniformly to the emitter-base junction, would result in the same collector and base currents.

$$I_n = J_{noo} \exp\left(\frac{q}{nkT} V_{un}\right) \pi r_E^2$$

$$I_C = J_{Coo} \exp\left(\frac{q}{kT} V_{un}\right) \pi r_E^2. \tag{20}$$

The excess voltage, ΔV_n, may be defined as

$$\Delta V_n = V_{BE} - V_{un}$$

$$= V_o + V(r_E) - V_{un}$$

$$= \frac{nkT}{q} \ell n\left(\frac{J_{no}}{J_{noo}}\right) + \frac{nkT}{q} \ell n\left[\frac{1}{\left(1 - \frac{q\rho_s J_{no}}{8\pi nkT}\pi r_E^2\right)^2}\right]$$

$$- \frac{nkT}{q} \ell n\left(\frac{I_n}{J_{no}\pi r_E^2}\right)$$

$$= \frac{nkT}{q} \ell n \frac{J_{no}\pi r_E^2/I_n}{\left(1 - \frac{q\rho_s J_{no}}{8\pi nkT}\pi r_E^2\right)^2}, \qquad (21)$$

where equations 12, 17, and 20, have been used.

Substituting equation 19 into equation 21, one obtains

$$\Delta V_n = \frac{nkT}{q} \ell n\left(1 + \frac{\rho_s}{8\pi}\frac{q}{nkT} I_n\right). \qquad (22)$$

Reference to a graph on semilog paper reveals that for a voltage deviation ΔV, $\exp\left(\frac{q}{kT}\Delta V\right)$ is the ratio of the collector current that would flow (were the sheet resistance negligibly small), I_{CI}, to the measured value of collector current, I_C. Both ΔV and I_{CI}/I_C may be determined experimentally.

$$\frac{I_{CI}}{I_C} = \exp\left(\frac{q}{kT}\Delta V_n\right)$$

$$= \left(1 + \frac{\rho_s}{8\pi}\frac{q}{nkT} I_n\right)^n. \qquad (23)$$

For n = 1, equation 23 becomes the solution found by Looney. From equation 23, observe that as I_n becomes greater than $\frac{8\pi nkT}{\rho_s q}$, we have

$$\frac{I_{CI}}{I_C} \rightarrow \left(\frac{\rho_s}{8\pi}\frac{q}{nkT}I_n\right)^n$$

$$= \left(\frac{\rho_s}{8\pi}\frac{q}{nkT}\right)^n I_n^n, \tag{24}$$

or

$$\log\left(\frac{I_{CI}}{I_C}\right) \rightarrow n \log\left(\frac{\rho_s}{8\pi}\frac{q}{nkT}\right) + n \log I_n, \tag{25a}$$

so that the limiting slope, that is, the derivative with respect to $\log(I_n)$, should approach n.

$$\frac{\partial \log\left(\frac{I_{CI}}{I_C}\right)}{\partial \log (I_n)} \rightarrow n. \tag{25b}$$

Figure 11 illustrates plots of experimental data for two representative devices for both the pre- and postirradiation characteristics. Note that on both sets of curves the plot of preirradiation data approaches a limiting slope of $n = 1$ indicating that in the unirradiated device the deviation of the current-voltage characteristic is caused by the bulk diffusion recombination-generation component of base current. This is further evidence for the assumption that the preirradiation "n = 1.5 component" of base current is of surface-perimeter origin since it does not contribute to the current-voltage deviation.

On both sets of curves the postirradiation data approach limiting slopes of $n = 1.5$, indicating that the neutron-induced anomalous current component is primarily responsible for the deviation of the current-voltage characteristics and that this component now originates primarily in the bulk space-charge region of the emitter-base junction.

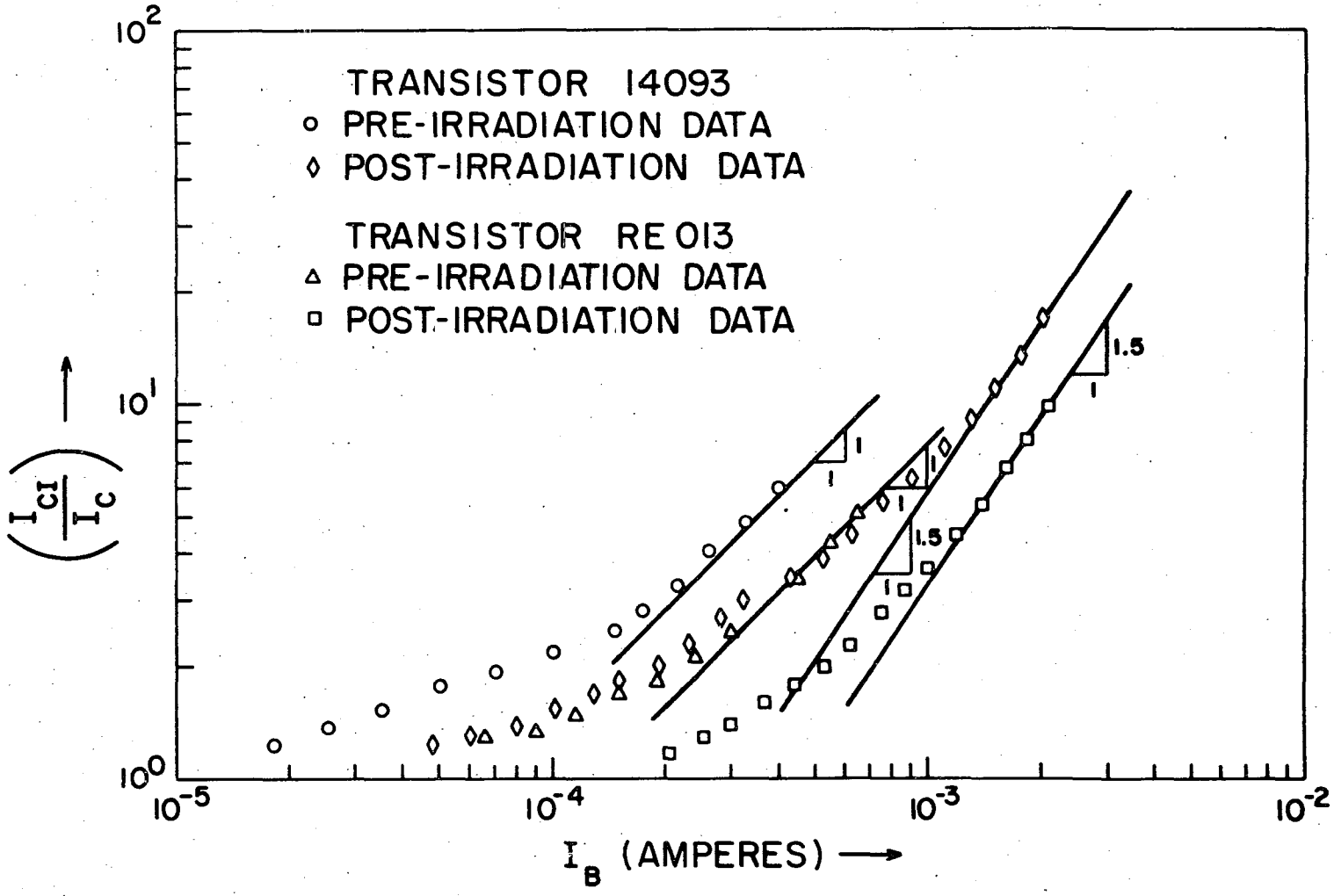

Figure 11. $\frac{I_{CI}}{I_C}$ vs I_B - limiting slopes for pre- and post-irradiation data

It is possible, from equations 24 and 25a, to consider the dependence of the current-voltage deviation on the applied voltage, V_{BE}.

The current, I_n, may be written as

$$I_n = \pi J_{noo} \exp\left(\frac{q}{kT} V_o\right) \int_0^{r_E} \exp\left(\frac{q}{nkT} V(r)\right) r dr, \tag{26}$$

or equivalently as

$$I_n = \pi r_E^2 J_{noo} \exp\left(\frac{q}{nkT} V_{un}\right), \tag{27}$$

but $V_{un} = V_{BE} - \Delta V_n$, so that

$$\begin{aligned} I_n &= \pi r_E^2 J_{noo} \exp\left(\frac{q}{nkT}(V_{BE} - \Delta V_n)\right) \\ &= \pi r_E^2 J_{noo} \exp\left(\frac{q}{nkT} V_{BE}\right) \cdot \exp\left(\frac{-q}{nkT} \Delta V_n\right) \\ &= \pi r_E^2 J_{noo} \exp\left(\frac{q}{nkT} V_{BE}\right) \cdot \left(\frac{I_C}{I_{CI}}\right)^{1/n} \end{aligned} \tag{28}$$

Substituting the last of equation 28 into equation 24, one obtains, for large deviations,

$$\left(\frac{I_{CI}}{I_C}\right) \rightarrow \left(\frac{\rho_s}{8\pi} \frac{q}{nkT}\right)^n \left(\pi r_E^2 J_{noo}\right)^n \exp\left(\frac{q}{kT} V_{BE}\right) \left(\frac{I_C}{I_{CI}}\right). \tag{29}$$

Solving equation 22 for $\frac{I_{CI}}{I_C}$ results in

$$\left(\frac{I_{CI}}{I_C}\right) = \left(\frac{\rho_s}{8\pi} \frac{q}{nkT}\right)^{n/2} \left(\pi r_E^2 J_{noo}\right)^{n/2} \exp\left(\frac{q}{2kT} V_{BE}\right). \tag{30}$$

Putting equation 30 in the form of equation 25,

$$\log\left(\frac{I_{CI}}{I_C}\right) = \frac{n}{2} \cdot \log\left(\frac{\rho_s}{8\pi}\frac{q}{nkT}\right) + \frac{n}{2} \cdot \log\left(\pi r_E^2 J_{noo}\right) + \frac{q}{2kT} V_{BE}. \qquad (31)$$

From equation 31, one sees that a plot $\frac{I_{CI}}{I_C}$ versus V_{BE} on semilog paper should approach a limiting slope of $\frac{q}{2kT}$. That is,

$$\frac{\partial \log\left(\frac{I_{CI}}{I_C}\right)}{\partial V_{BE}} \rightarrow \frac{q}{2kT} \qquad (32)$$

as V_{BE} increases, and this is true for either component of current dominating the current-voltage deviation. The intercept of the limiting slope increases with irradiation, i.e., as n changes from 1 to 1.5.

From Figure 12, which consists of plots of $\frac{I_{CI}}{I_C}$ versus V_{BE} for pre- and postirradiation experimental data, it may be seen that the above statements are correct.

As may be inferred from the above derivations, the values of the sheet resistivity, ρ_s, may be obtained from curves of $\frac{I_{CI}}{I_C}$ versus I_n. The values so obtained range from 30 percent less than to 30 percent more than the values of sheet resistivity obtained from measurements on the double-base and Hall-effect structures. Since the value obtained for ρ_s from these curves is very sensitive to the placement of the straight-line asymptotes with respect to the data points, this is considered to be reasonable agreement.

F. Double-Base Transistors

On the double-base transistors the conventional current-voltage characteristics were measured as a function of the base 1-to-base 2 bias.

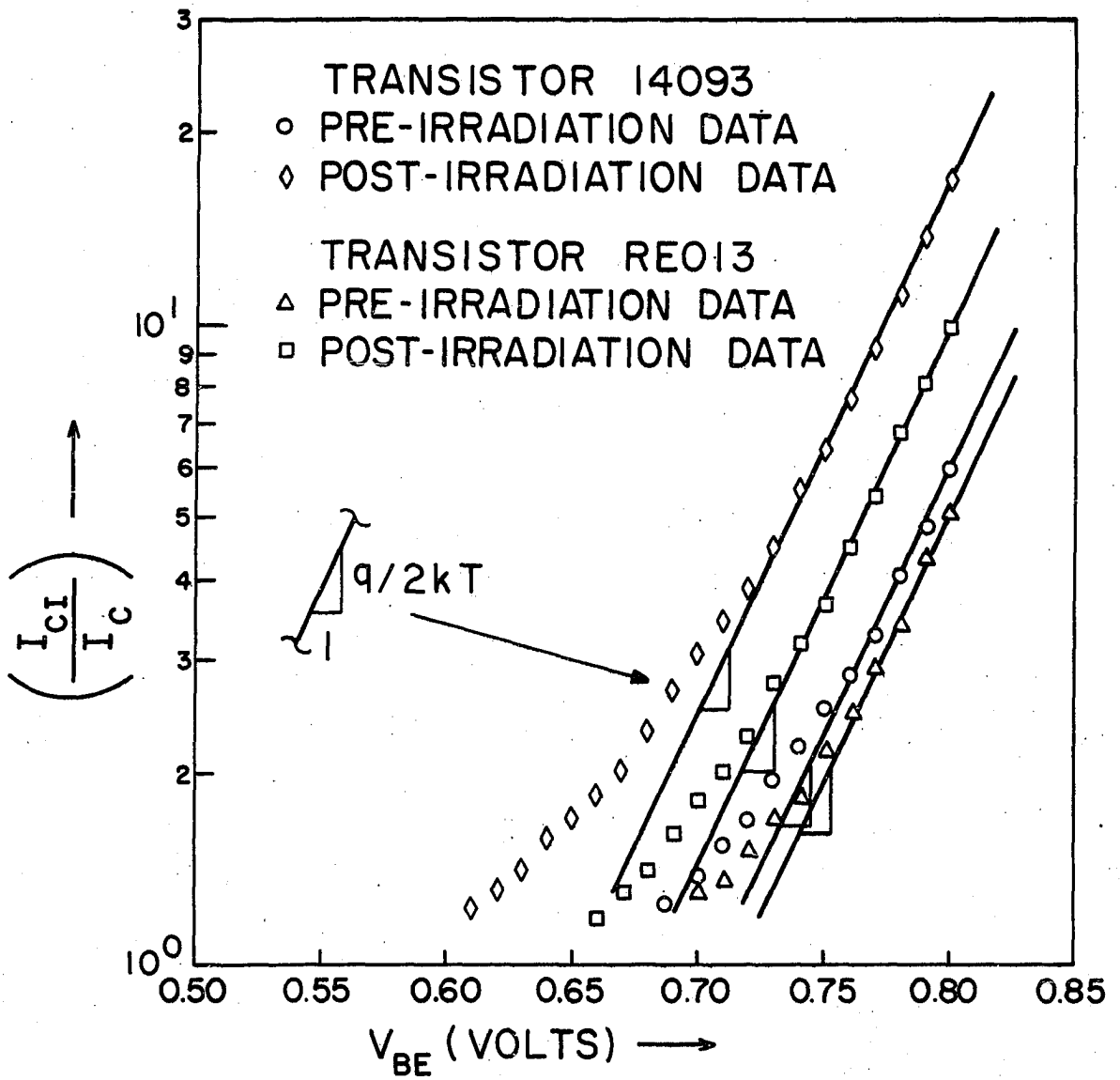

Figure 12. $\frac{I_{CI}}{I_C}$ vs V_{BE} - limiting slopes for pre- and post-irradiation data

This bias was observed to affect only the magnitude of the base current and not its slope. Also measured on the double-base transistors was the sheet resistivity, which was incorporated with the sheet resistivity measured on Hall-effect devices.

G. Effect of Transverse Biasing on the Double-Base Transistor

Consider a double-base transistor with the geometry shown in Figure 13. Assume that the applied emitter-to-base bias, V_{BE}, is constant and is of such magnitude ($0.3V \leq V_{BE} \leq 0.6V$) that the "1.5 component" of current is dominating the base current. For V_{BE} in the range indicated, the transverse biasing effects of the base current as it flows from under the emitter to the base contacts will be negligible.

For an externally applied base 1-to-base 2 potential, V_{12}, the potential at any point r is V_{BE} plus the contribution due to V_{12}. Hence,

$$V(r) = V_{BE} - \frac{V_{12}}{\ell n \frac{r_2}{r_1}} \ell n \left(\frac{r}{r_1} \right). \tag{33}$$

Consider now two different and distinct possibilities for the origin of the "1.5 component" of current.

Case 1 -- This component may arise at the perimeter of the emitter-base junction where the junction intersects the surface and, hence, is a surface-perimeter current as identified by Iwersen (7) and Coppen and Matzen (8) for unirradiated transistors.

Case 2 -- This component may arise primarily in the bulk space-charge region of the emitter-base junction, as appears to be the situation after neutron bombardment to some reasonable flux level.

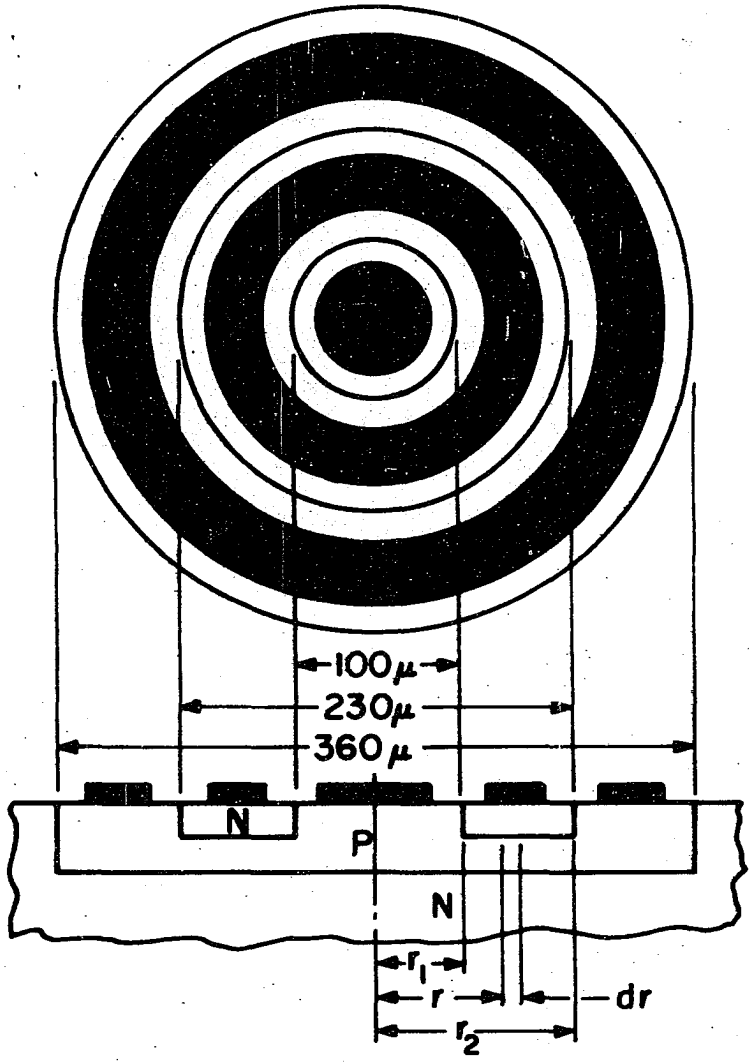

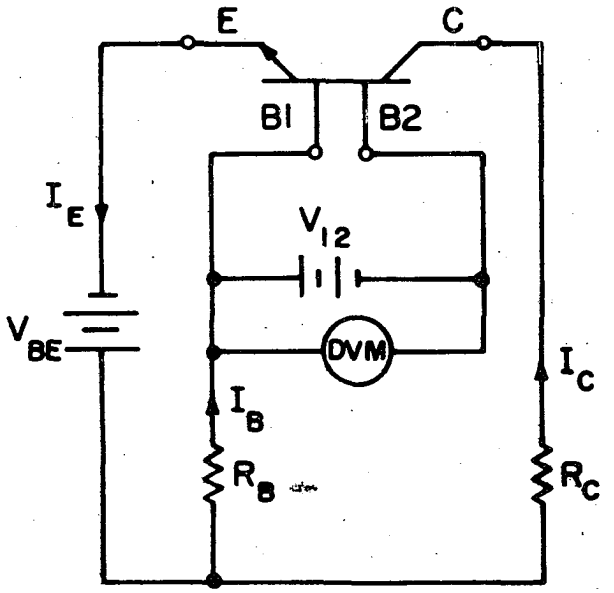

R_C AND R_B ARE CURRENT SAMPLING RESISTORS

V_{BE} AND V_{12} ARE JOHN FLUKE I/V CALIBRATORS

Figure 13. Geometry of double base transistor and biasing scheme

First consider Case 1, subject to the condition that $0.3\,V \leq V_{BE} \leq 0.6\,V$, so that the ideal component of base current is much less than the "n = 1.5 component". That is,

$$I_B(n = 1) = \int_{r_1}^{r_2} J_{B10} \exp\left(\frac{q}{kT} V(r)\right) 2\pi r dr \ll I_B(n = 1.5) \approx I_B. \tag{34}$$

The "n = 1.5 component" for Case 1 is given by the expression

$$I_B \approx I_B(n = 1.5) = J_{no\ell}\left[2\pi r_1 \exp\left(\frac{q}{nkT} V(r_1)\right) + 2\pi r_2 \exp\left(\frac{q}{nkT} V(r_2)\right)\right], \tag{35}$$

where $J_{no\ell}$ is the linear current density at the emitter perimeter where the base-emitter junction intersects the surface of the semiconductor die. From equation 33, the potential at the inner and outer radii of the emitter may be evaluated as

$$\begin{aligned} V(r_1) &= V_{BE} \\ V(r_2) &= V_{BE} - V_{12} \\ &= V_{BE} + V_{21}. \end{aligned} \tag{36}$$

Note that, for V_{21} positive and large in magnitude the outer perimeter will be heavily forward biased, and, for V_{21} negative and large in magnitude the outer perimeter will be biased into cutoff or even reverse biased. Mathematically this may be written as

$$I_B = 2\pi J_{no\ell} \cdot \exp\left(\frac{q}{nkT} V_{BE}\right)\left\{r_1 + r_2 \exp\left(\frac{q}{nkT} V_{21}\right)\right\} \tag{37}$$

If one considers the ratio of $I_B(V_{21})$ to $I_B(0)$ at constant base-emitter bias, then the unknown quantity $J_{no\ell}$ drops out.

$$\frac{I_B(V_{21})}{I_B(0)} = \frac{r_1 + r_2 \exp\left(\frac{q}{nkT} V_{21}\right)}{r_1 + r_2}. \tag{38}$$

It may be seen from equation 38 that a plot of

$\left(\frac{I_B(V_{21})}{I_B(0)} - \frac{r_1}{r_1 + r_2}\right)$ versus V_{21} on semilog paper should be a straight line with intercept of $\frac{r_2}{r_1 + r_2}$ at $V_{21} = 0$ and slope of $\frac{q}{nkT}$, or a reciprocal slope of $\frac{nkT}{q}$(90 mv/decade). Hence, to verify that the "1.5 component" in the preirradiation case arises at the perimeter of the emitter-base junction, one would need only to plot the data indicated above.

Consider the second case, where the "n = 1.5 component" of base current is assumed to arise in the bulk space-charge region of the emitter-base junction. The base current in this case becomes

$$I_B \approx I_B(n = 1.5) = \int_{r_1}^{r_2} J_{no} \exp\left(\frac{q}{nkT} V(r)\right) 2\pi r dr. \tag{39}$$

When V(r) is given by equation 33, equation 39 may be rewritten as

$$I_B = 2\pi J_{no} \exp\left(\frac{q}{nkT} V_{BE}\right) \int_{r_1}^{r_2} \exp\left[\frac{q}{nkT} \frac{V_{21}}{\ell n \frac{r_2}{r_1}} \ell n\left(\frac{r}{r_1}\right)\right] r dr. \tag{40}$$

To get this integral into suitable form, let

$$a = \frac{q}{nkT} \frac{1}{\ell n\left(\frac{r_2}{r_1}\right)}, \quad x = \frac{r}{r_1},$$

and note that $\exp(c \cdot \ell n(x)) = x^c$; then,

$$I_B = 2\pi r_1^2 J_{no} \exp\left(\frac{q}{kT} V_{BE}\right) \int_1^{r_2/r_1} x^{(1+aV_{21})} dx$$

$$= 2\pi r_1^2 J_{no} \exp\left(\frac{q}{kT} V_{BE}\right) \left[\frac{\left(\frac{r_2}{r_1}\right)^{2+aV_{21}} - 1}{2 + aV_{21}}\right]. \qquad (41)$$

As in Case 1, consider the dimensionless ratio $\frac{I_B(V_{21})}{I_B(0)}$.

$$\frac{I_B(V_{21})}{I_B(0)} = \frac{2}{\left(\frac{r_2}{r_1}\right)^2 - 1} \cdot \frac{\left(\frac{r_2}{r_1}\right)^{2+aV_{21}} - 1}{2 + aV_{21}} \cdot \qquad (42)$$

For the assumption of bulk origin of the "n = 1.5 component", the ratio $\frac{I_B(V_{21})}{I_B(0)}$ varies less rapidly with base-to-base bias, V_{21}, than does the ratio for the assumption of surface-perimeter origin, as may be seen by comparing equations 38 and 42.

It seems logical, then, to prepare graphs of equations 38 and 42 on semilog paper and plot on this graph the experimental variations of $\frac{I_B(V_{21})}{I_B(0)}$ for comparison. Figure 14 is such a plot. The lines represent the theoretical calculations of equations 38 and 42, and the points

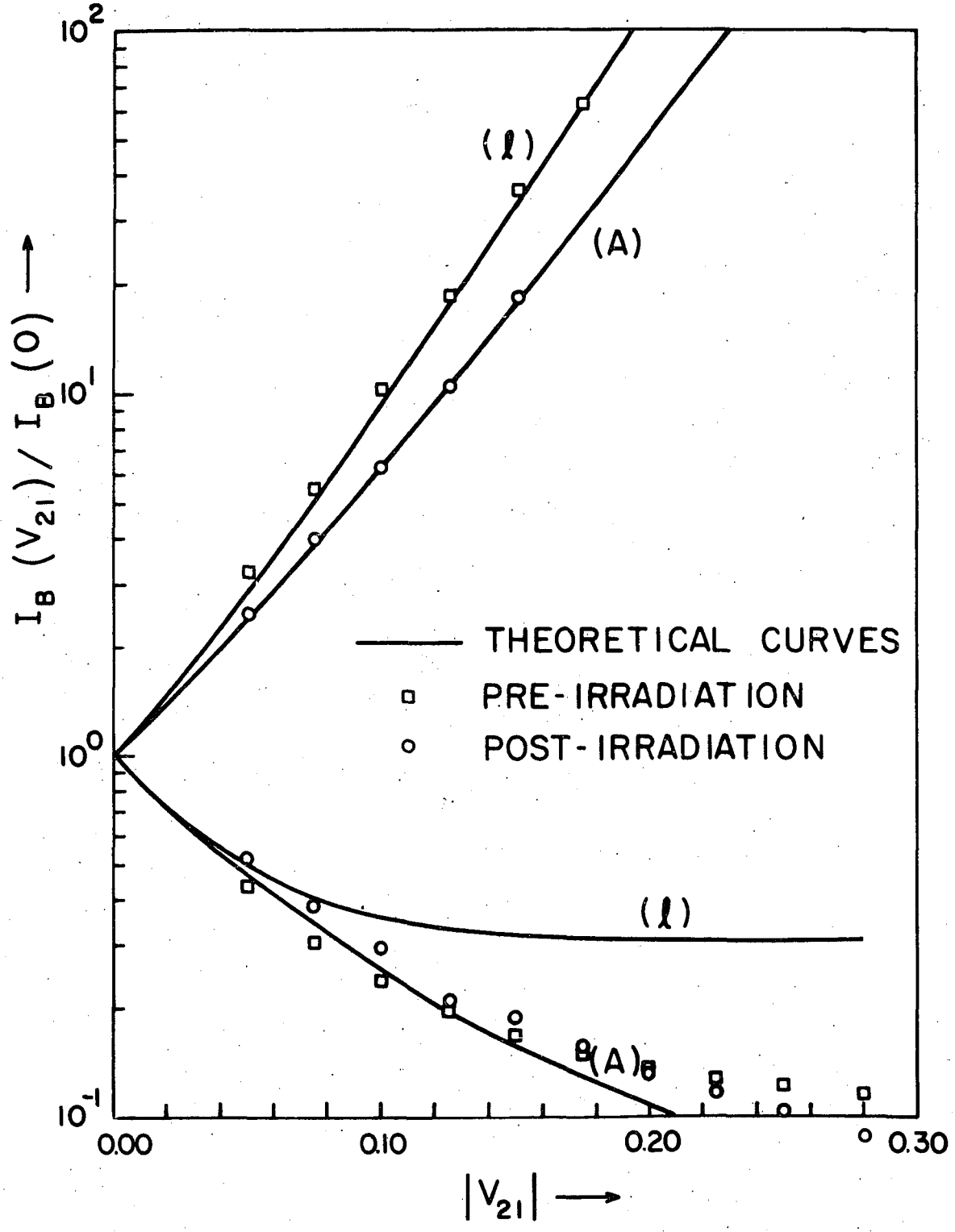

Figure 14. Comparison of theoretical calculations and experimental data

represent experimental data. In the forward bias situation ($V_{21} > 0$, upper curves), the preirradiation data follow closely the curve ℓ, which assumes surface-perimeter origin of the "1.5 component" of base current, while the postirradiation data follow closely the curve A, which assumes area dependence or bulk origin for the "1.5 component". The situation under reverse bias ($V_{21} < 0$, lower curves) is complicated by noise, but the general relations predicted by the theory (i.e., saturation for perimeter dependence (preirradiation data), nonsaturation for area dependence (postirradiation data)) are observed to hold.

H. Hall-Effect Transistors

The Hall constant, R_H, and sheet resistance, ρ_s, were measured on the Hall-effect devices, and the sheet resistance was combined with the sheet-resistance measurement on the double-base transistors to obtain average values. The results of these measurements are shown in Figure 15. Note that all the measurements are normalized so that one actually is looking at percentage changes in the parameters. Changes in mobility with irradiation are obtained from changes in the ratio of the Hall constant to the sheet resistance, since this gives the Hall mobility, which can be assumed to be proportional to the majority carrier mobility as well as to the minority carrier mobility. Changes in the number of majority carriers per unit area are obtained from the increased Hall constant. Each point in Figure 15 represents an average of the normalized values of all the devices in the group at each flux level. A 5-percent decrease in the average carrier concentration is obtained at a flux of about 4×10^{14} neutrons/cm^2, and corresponds reasonably well with values derived from carrier removal rates measured on bulk silicon by Stein (59). The 3-percent decrease in majority carrier mobility, which is the hole mobility, agrees with data taken by Wertheim (60) on bulk silicon. This figure reveals that, even at the highest flux levels, the ratio of the

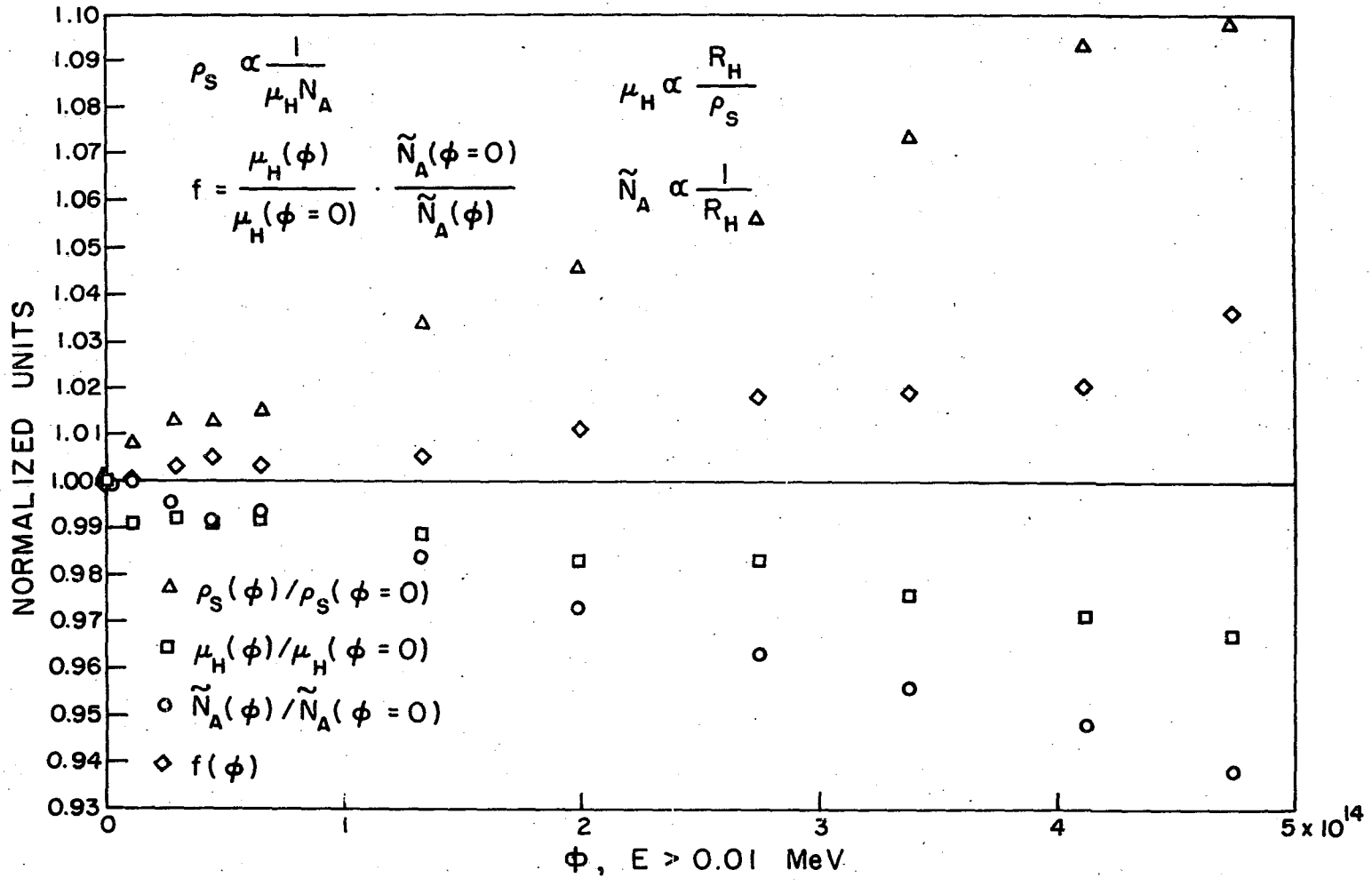

Figure 15. Normalized base region parameters vs ϕ

minority carrier mobility to the sheet carrier density, changed by only about 2 percent, so that indeed the change in collector current with irradiation is primarily associated with the reduction in the base recombination term (See equation 7).

I. Emitter Efficiency and Base Recombination Term in Neutron Irradiated Transistors

As noted in the introduction, it has been stated in the literature that the emitter efficiency in neutron-irradiated transistors is not a function of integrated neutron flux and was assumed constant for all levels of flux (2 - 6). The same papers have attributed the decrease in transistor current gain only to a decrease in lifetime of minority carriers in the bulk base region, that is, to a decrease in the base recombination term. The base recombination term is defined here, as is usual, as the ratio of the injected minority carrier current on the collector side of the base to the injected minority carrier current on the emitter side of the base. The preceding sections have shown that the decrease in the base recombination term at low and intermediate current levels is only a small fraction of the decrease in common-base current gain, and that the major fraction of the decrease in current gain is due to a neutron-induced component of base current which acts to decrease the transistor current gain by decreasing the emitter efficiency. The emitter efficiency is defined here, as is usual, as the ratio of the injected minority carrier current at the emitter side of the base to the total current flowing in the emitter.

1. Emitter efficiency

This section presents a detailed analysis of the emitter efficiency and presents two equations for the determination of emitter efficiency as a function of integrated neutron flux from preirradiation measurements on a device. The first of these is an exact equation, while the second

equation is an approximation which is valid for all ranges of neutron flux less than a few times 10^{14} neutrons/cm^2. The approximation deviates by much less than 2 percent from the exact equation, and deviates only at small values of flux, where degradation is small, at extremely high values of emitter-base voltage where the normal transistor relationships begin to break down because of the fringing of the injected emitter current and conductivity modulation, that is, in the high-current-level regime at low flux levels.

Figure 16 shows a schematic diagram of the currents flowing in a transistor. The first of these is the injected electron current (for an NPN device). This current component may be approximated as (10)

$$I_{EN} = \frac{kTA_E n_i^2 \mu_n}{\widetilde{N}_A} \exp\left(\frac{q}{kT} V_{BE}\right), \tag{43}$$

where the quantities are as previously defined. The approximation is valid for the diffusion length of minority carriers large with respect to the base width, which is nearly always the case in modern "drift" transistors.

One may consider, in addition, the variation of these components with integrated neutron flux, ϕ. In the above expression, the quantities which vary with ϕ are the minority carrier mobility and sheet density. Hence, the equation for the injected electron current may be rewritten to show this variation with ϕ more explicitly. Dividing and multiplying numerator and denominator by unity, one obtains

$$I_{EN}(V_{BE}, \phi) = \frac{kTA_E n_i^2 \mu_n(\phi = 0)}{\widetilde{N}_A(\phi = 0)} \cdot \frac{\mu_n(\phi)/\mu_n(\phi = 0)}{\widetilde{N}_A(\phi)/\widetilde{N}_A(\phi = 0)} \cdot \exp\left(\frac{q}{kT} V_{BE}\right). \tag{44}$$

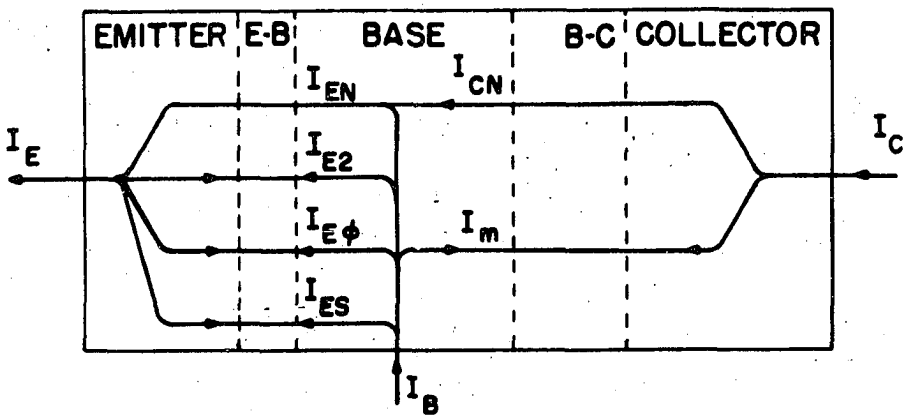

I_{EN} = INJECTED ELECTRON CURRENT

$$\propto \exp\left(\frac{q}{kT} V_{BE}\right)$$

I_{CN} = COLLECTED ELECTRON CURRENT

$$= \beta \cdot I_{EN}$$

I_m = COLLECTOR MULTIPLICATION CURRENT

$$= (\alpha^* - 1) I_{CN}$$

I_{E2} = NORMAL SPACE CHARGE RECOMBINATION CURRENT

$$\propto \exp\left(\frac{q}{2kT} V_{BE}\right)$$

I_{ES} = SURFACE-PERIMETER RECOMBINATION CURRENT

$$\propto \exp\left(\frac{q}{nkT} V_{BE}\right), \quad n \approx 1.5$$

$I_{E\phi}$ = NEUTRON-INDUCED RECOMBINATION CURRENT

$$= A_E \cdot K_1 \cdot \phi \cdot \exp\left(\frac{q}{nkT} V_{BE}\right), \quad n \approx 1.5$$

Figure 16. Components of current flowing in a p-n junction transistor after exposure to neutron irradiation

Also it is known that the ratio of the minority and majority carrier mobilities is approximately a constant, that is,

$$\frac{\mu_n}{\mu_p} \approx b, \tag{45}$$

so that the equation for I_{EN} may be rewritten as

$$I_{EN}(V_{BE}, \phi) = \frac{kTA_E n_i^2 \mu_{no}}{\tilde{N}_{A0}} \cdot \frac{\mu_p(\phi)/\mu_{po}}{\tilde{N}_A(\phi)/\tilde{N}_{A0}} \cdot \exp\left(\frac{q}{kT} V_{BE}\right), \tag{46}$$

where the subscript 0 indicates $\phi = 0$. Furthermore, the majority carrier mobility, μ_p, is proportional to the Hall mobility, μ_H;

$$\mu_p \propto \mu_H, \tag{47}$$

which in turn is equal to the ratio of the Hall constant, R_H, to the sheet resistance, ρ_s;

$$\mu_H = R_H/\rho_s. \tag{48}$$

The sheet resistance is inversely proportional to the product of the majority carrier mobility and the sheet carrier density.

$$\rho_s \propto \frac{1}{\mu_H \tilde{N}_A} \tag{49}$$

Using these relationships, one may again rewrite I_{EN} as

$$I_{EN} = \frac{kTA_E n_i^2 \mu_{no}}{\tilde{N}_{A0}} \cdot \frac{\left(R_H(\phi)/R_{H0}\right)^2}{\rho_s(\phi)/\rho_{so}} \cdot \exp\left(\frac{q}{kT} V_{BE}\right) \tag{50}$$

or

$$I_{EN} = f(\phi) \cdot I'_{EN0} \cdot \exp\left(\frac{q}{kT} V_{BE}\right) \tag{51}$$

where the functions $f(\phi)$ and I'_{EN0} are defined by

$$f(\phi) = \left(R_H(\phi)/R_{H0}\right)^2 / \left(\rho_s(\phi)/\rho_{so}\right)$$

$$I'_{EN0} = \frac{kTA_E n_i^2 \mu_{no}}{\tilde{N}_{A0}} \tag{52}$$

The function $f(\phi)$ has previously been determined as a function of flux and is plotted in Figure 15. Note that $f(\phi)$ deviates from unity by, at most, about 2 percent out to an integrated flux of 4×10^{14} neutrons/cm^2.

The normal, or Sah-Noyce-Shockley, bulk space charge recombination current is given by

$$I_{E2} = I_{E20} \exp\left(\frac{q}{2kT} V_{BE}\right). \tag{53}$$

This component is appreciable only at very small emitter-base voltages and apparently originates from the distribution of recombination centers in the space charge region (12). This "n = 2.0 component" of p-n junction current depends on the limiting lifetimes in the junction and has been observed to change only slightly with neutron irradiation (29), and so may be assumed a constant with respect to flux.

The current component, I_{Es}, is the current flowing at, or just under, the surface due to surface recombination where the emitter-base junction intersects the surface, that is, at the perimeter of the emitter. This component of current may arise from the recombination centers caused by the precipitation of impurity atoms in the highly doped area where the emitter and base diffusions intersect each other and the surface. The current component, I_{Es}, varies with voltage as

$$I_{Es} = I_{Es0} \exp\left(\frac{q}{nkT} V_{BE}\right), \tag{54}$$

where n is approximately 1.5.

The surface channel recombination-generation current, I_{Em}, varies as

$$I_{Em} = I_{Em0} \exp\left(\frac{q}{mkT} V_{BE}\right), \tag{55}$$

where m is normally between 2 and 4, although larger values have been noted for large channels (7, 11). The current component, I_{Em}, is negligible on surface-passivated silicon transistors.

Since the observed surface effects of neutron irradiation have been small, both the I_{Es} and I_{Em} components of p-n junction current may be assumed constant with respect to integrated neutron flux.

The multiplication current, I_m, is normally negligible in silicon at low collector-base biases. The current component, I_m, is given by the equation

$$I_m = (\alpha^* - 1) I_{CN}, \tag{56}$$

where α^* is the collector multiplication factor. The current multipication term, $(\alpha^* - 1)$, is normally much less than 10^{-3} for silicon devices (61) biased far below the breakdown voltage for the collector-base junction.

The component of current, $I_{E\phi}$, exists only in irradiated transistors and is given to first order, by work from the previous sections, as

$$I_{E\phi} = K_1 \cdot A_E \cdot \phi \cdot \exp\left(\frac{q}{nkT} V_{BE}\right). \tag{57}$$

where the definition of the symbols employed are repeated below for clarity.

A_E is the emitter area,

ϕ is the integrated neutron flux,
K_1 is equal to 3.33×10^{-22} (amperes/cm^2)/(neutron/cm^2), and
n is approximately 1.5.

The emitter efficiency is the ratio of the injected minority carrier current on the emitter side of the base to the total current flowing in the emitter circuit. Hence, the following equation must hold.

$$\gamma = \frac{I_{EN}}{I_{EN} + I_{E2} + I_{Em} + I_{Es} + I_{E\phi}} . \tag{58}$$

Rewriting this last equation in terms of applied voltage across the emitter-base junction, V_{BE}, and the integrated neutron flux, ϕ, the following equation results.

$$\gamma(V_{BE}, \phi) = \left[f(\phi) \cdot I'_{EN0} \cdot \exp\left(\frac{q}{kT} V_{BE}\right) \right] \div \left[f(\phi) \cdot I'_{EN0} \cdot \exp\left(\frac{q}{kT} V_{BE}\right) + I_{E20} \cdot \exp\left(\frac{q}{2kT} V_{BE}\right) + I_{Emo} \cdot \exp\left(\frac{q}{mkT} V_{BE}\right) + I_{Eso} \exp\left(\frac{q}{1.5kT} V_{BE}\right) + K_1 \cdot A_E \cdot \phi \cdot \exp\left(\frac{q}{1.5kT} V_{BE}\right) \right] . \tag{59}$$

The emitter efficiency may be normalized to its preirradiation value, $\gamma(V_{BE}, \phi = 0)$, which differs from the above equation only in that $f(\phi = 0)$ is replaced by unity, and the last term in the denominator by zero. Hence, dividing numerators and denominators separately,

$$\frac{\gamma(V_{BE}, \phi)}{\gamma_o(V_{BE})} = f(\phi) \div \left\{ \left[f(\phi) \cdot I'_{EN0} \cdot \exp\left(\frac{q}{kT} V_{BE}\right) + I_{E2} + I_{Em} + I_{Es} + K_1 \cdot A_E \cdot \phi \cdot \exp\left(\frac{q}{nkT} V_{BE}\right) \right] / I_E\left(V_{BE}, \phi = 0\right) \right\} \tag{60}$$

where the denominator of $\gamma(V_{BE}, \phi = 0) = \gamma_o(V_{BE})$ has been replaced by $I_E(V_{BE}, \phi = 0)$. Replacing the first four terms in the denominator of $\gamma(V_{BE}, \phi)$ by $I_E(V_{BE}, \phi = 0) + \left[f(\phi) - 1\right] \cdot I_{EN0} \exp\left(\frac{q}{kT} V_{BE}\right)$, the preceding equation becomes

$$\frac{\gamma(V_{BE}, \phi)}{\gamma_o(V_{BE})} = f(\phi) \div \left[1 + \frac{\left(f(\phi) - 1\right) \cdot I_{EN0} \cdot \exp\left(\frac{q}{kT} V_{BE}\right)}{I_E(V_{BE}, \phi = 0)} + \frac{K_1 \cdot A_E \cdot \phi \cdot \exp\left(\frac{q}{nkT} V_{BE}\right)}{I_E(V_{BE}, \phi = 0)}\right] . \tag{61}$$

Now, to make the equation independent of area, the currents are replaced by current density, since the areas cancel.

$$\frac{\gamma(V_{BE}, \phi)}{\gamma_o(V_{BE})} = f(\phi) \div \left[1 + \frac{\left(f(\phi) - 1\right) \cdot J_{EN0} \cdot \exp\left(\frac{q}{kT} V_{BE}\right)}{J_E(V_{BE}, \phi = 0)} + \frac{K_1 \cdot \phi \cdot \exp\left(\frac{q}{nkT} V_{BE}\right)}{J_E(V_{BE}, \phi = 0)}\right] . \tag{62}$$

The above equation is an exact relation for the normalized emitter efficiency. It may be converted into a more usable form by approximating the second term in the denominator by zero. To justify this, note that $J_{EN0} \exp\left(\frac{q}{kT} V_{BE}\right) / J_E(V_{BE}, \phi = 0)$ is just the initial emitter efficiency, $\gamma_o(V_{BE})$, and hence must be always less than unity for any applied voltage. Hence the second term in the denominator is always less than $(f(\phi) - 1)$.

Figure 15 shows that $f(\phi)$ is close to unity for small values of ϕ, and that at large values of ϕ, where the third term in the denominator begins to dominate, $f(\phi)$ differs from unity by about 0.02. Thus, for the worst

case, the maximum error in approximating the normalized emitter efficiency by

$$\frac{\gamma(V_{BE},\ \phi)}{\gamma_o(V_{BE})} \approx f(\phi) \div \left\{1 + \frac{K_1 \cdot \phi \cdot \exp\left(\frac{q}{nkT} V_{BE}\right)}{J_E(V_{BE},\ \phi = 0)}\right\} \tag{63}$$

is much less than 2 percent at large emitter-base bias voltages and low and intermediate values of flux, and decreases as either the emitter-base voltage is decreased or the neutron flux is increased.

2. Base recombination term

As indicated earlier, the collector current may be approximated as

$$I_C = \beta \cdot \frac{\mu_n}{\tilde{N}_A} \cdot n_i^2 \cdot kT \cdot \exp\left(\frac{q}{kT} V_{BE}\right), \tag{64}$$

so that the normalized base recombination term may be shown to be given by

$$\frac{\beta(\phi)}{\beta(\phi = 0)} = \frac{I_C(\phi)}{I_C(\phi = 0)} \cdot \frac{\tilde{N}_A(\phi)}{\tilde{N}_A(\phi = 0)} \cdot \frac{\mu_n(\phi = 0)}{\mu_n(\phi)} \tag{65}$$

Figure 17 displays curves of normalized base recombination term and normalized emitter efficiency versus integrated neutron flux. The topmost curve is the base recombination term and is voltage independent, and the lower curves are emitter efficiency versus integrated flux for four different emitter-base bias conditions.

Since the common-base current gain is the product of emitter efficiency and base recombination term, it is apparent from Figure 17 that the emitter efficiency, which has been assumed by previous workers (2 - 6) to be equal to a constant for all values of flux, is indeed responsible for a large fraction of the degradation in common-base current gain at

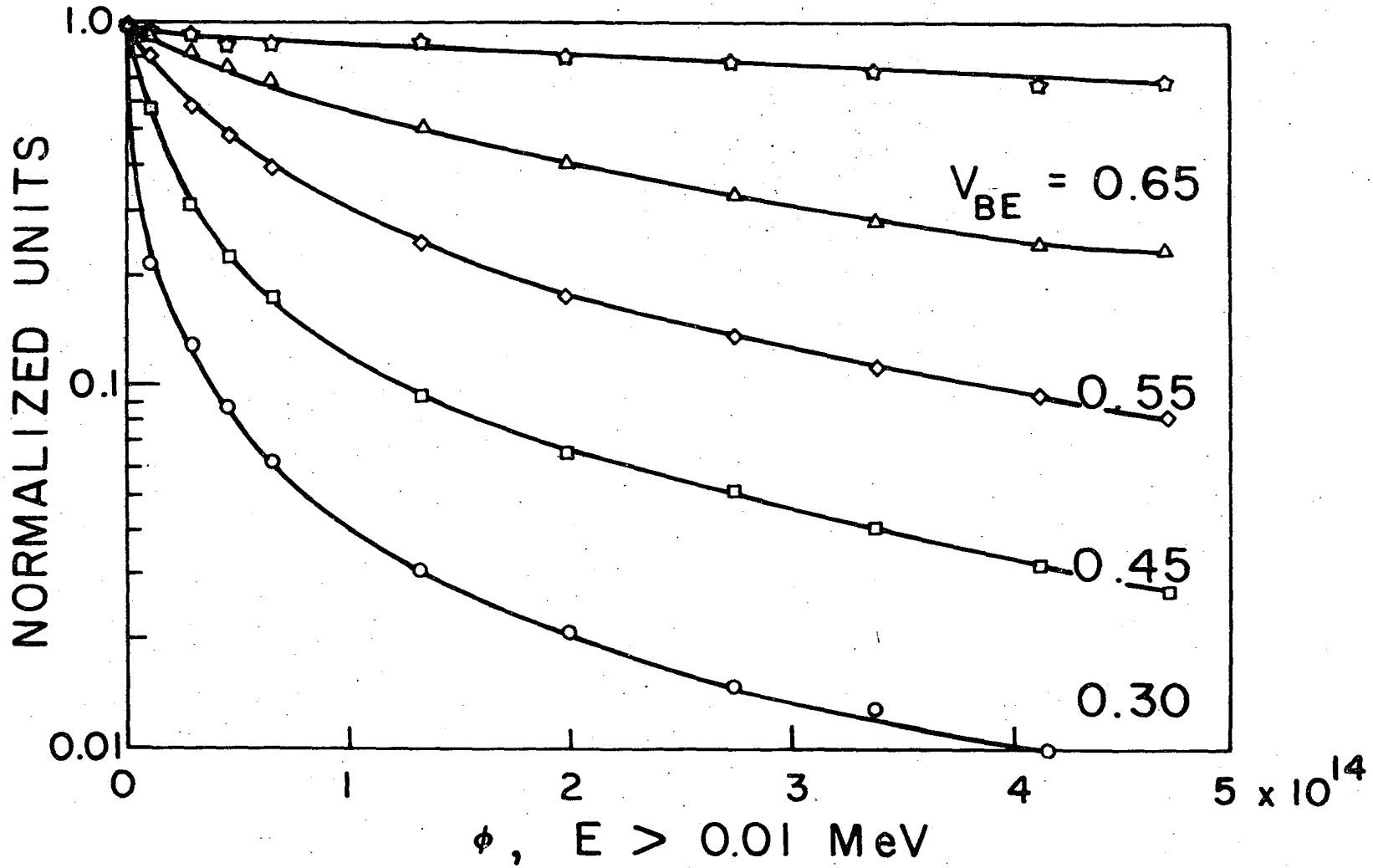

Figure 17. Ratios of emitter efficiencies and base recombination term vs ϕ

low and intermediate current levels, while the base recombination term contributes only a small fraction to the degradation.

The more familiar common-emitter current gain (h_{FE}) may be derived from the common-base current gain (α) by

$$h_{FE} = \frac{\alpha}{1 - \alpha} \quad . \tag{66}$$

The conclusions reached for the common-base current gain will certainly hold for the common-emitter current gain.

J. Search for the Anomalous Component of Current in Other Structures

To test the validity of these results on other transistor structures, a group of low-frequency PNP alloy silicon transistors were irradiated to 2.6×10^{11} and 1.2×10^{12} neutrons per square centimeter. These lower levels were chosen because alloy transistors are more sensitive to neutron irradiation than are diffused devices. The incremental changes in base current were plotted versus emitter-base voltage. Slopes of these plots were found to correspond quite closely to an n of 1.5 with a maximum spread of ±20 percent. Additionally, several types of NPN silicon transistors, including planar, planar epitaxial, mesa, diffused, and grown-diffused devices, were irradiated by increments to destruction. The incremental change in base current at each flux level was plotted as a function of base-emitter voltage and again was found to have slopes corresponding closely to an n of 1.5 with maximum spread of ±20 percent.

K. Temperature Dependence and Annealing of the Anomalous Component of Current

In the course of completing the experiments described in the preceding sections, the devices were irradiated in increments to a total

integrated flux of about 7×10^{14} neutrons/cm^2. One may now consider the question: How does this neutron-induced component of current behave as a function of temperature, and what are the characteristics of the devices after annealing has taken place?

In silicon, substantial annealing takes place at 40°C to 50°C. It is possible, therefore, to examine the current-voltage characteristics as a function of temperature only for temperatures below this limit before annealing begins.

The device characteristics for the group of devices were measured at 27°C, 0°C, -25°C, and -50°C. The n of the reciprocal slope term, nkT/q, was observed to increase with decreasing temperature from approximately 1.5 at room temperature to 1.6 to 1.7 at -50°C.

The devices were then annealed for 4 hours at 150°C. This time is somewhat longer than necessary to complete the annealing, and was made so deliberately to avoid the possibility of further annealing taking place during measurements at elevated temperatures.

The device characteristics were then measured at -50°C, -25°C, 0°C, 27°C, 50°C, 75°C, and 100°C.

The n of the reciprocal slope term, nkT/q, was about 1.6 at -50°C, decreased to approximately 1.5 at room temperature (27°C), and decreased further as the temperature was increased to about 1.3 at 100°C.

The device characteristics after annealing showed definite improvement in both the collector- and base-current characteristics. The base current, which had increased rapidly with neutron bombardment, shifted down about half an order of magnitude. The collector current, which had decreased slowly with neutron flux, shifted upwards towards its preirradiation value. Figure 18 displays the pre- and postannealing characteristics for a typical device. The solid lines in the figure represent the

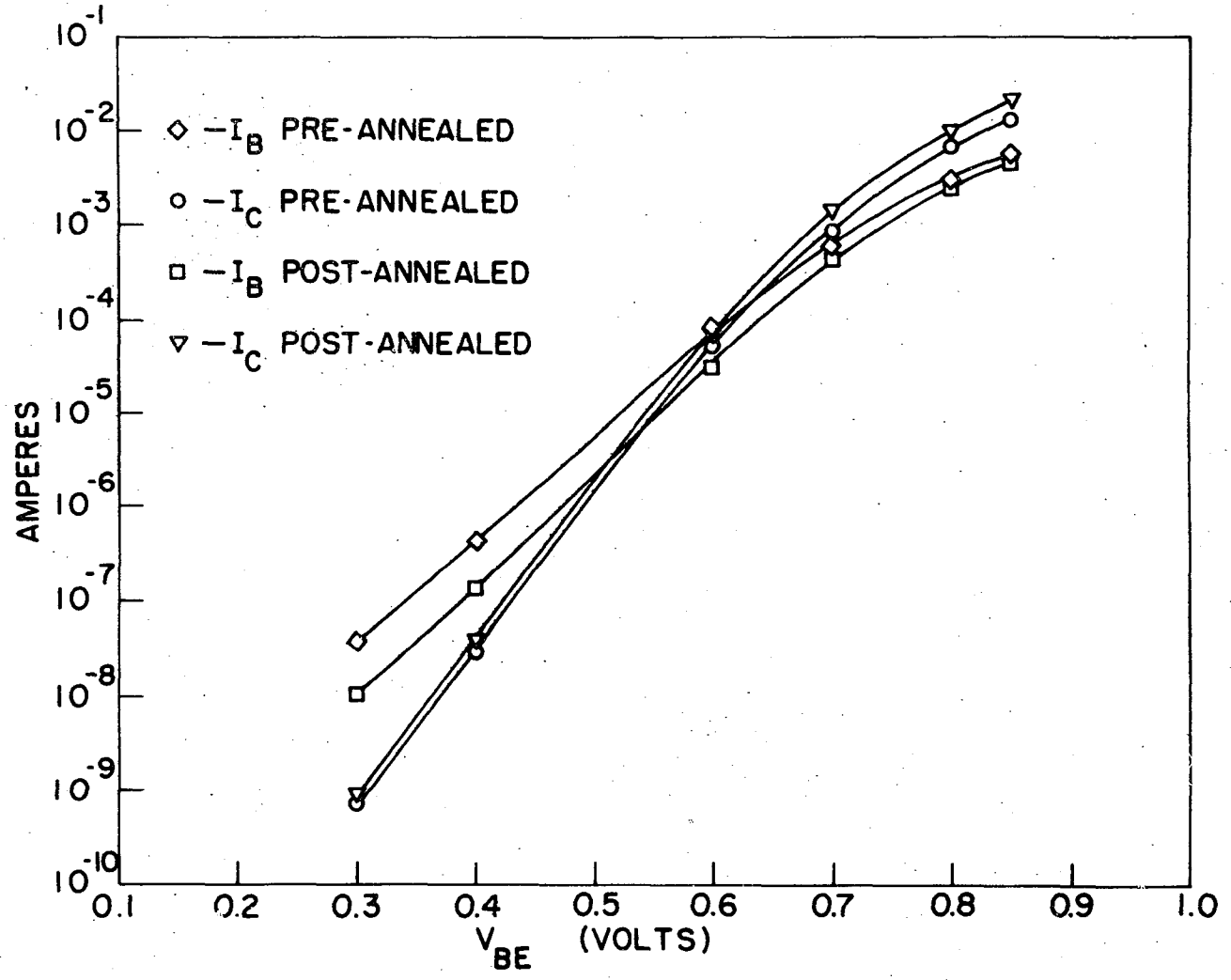

Figure 18. Pre- and post-annealing I-V characteristics

data points which were taken at 10-millivolt increments. The symbols are for identification of the curves.

Comparison of the room-temperature current-voltage characteristic after annealing with current-voltage characteristics measured on the same devices at lower flux levels revealed that the base-current characteristic coincided approximately with data taken at a flux level of 2×10^{14} *neutrons/cm*^{2}. The annealed collector-current characteristics, however, coincided with its preirradiation-level characteristic at low- and intermediate-current levels and deviated below its preirradiation-level characteristic at higher current levels. This is due to the base current's being much larger than in the preirradiated situation, thereby causing a much larger transverse voltage drop. Figure 19 displays curves of the type discussed for a typical device.

Since the base current arises, for the most part, in the emitter-base space-charge region, the different effects of annealing on the base current and collector current (which depend on bulk recombination) would seem to indicate different annealing rates for the neutral bulk base region and the high field region of the emitter-base space-charge region.

L. Possible Explanation of the Origin of the Anomalous Component of Current

Iwersen (7) and Coppen and Matzen (8) independently found that a "1.5 component" of current is responsible for the falloff of transistor current gain with decreasing current density. Both concluded that this "1.5 component" of current was due to recombination at, or just under, the surface in the region where the emitter-base junction intersects the surface. This result has been verified in this laboratory. It is known that clusters (aggregates), or microcrystals, of impurity atoms precipitate out in a diffused region close to the surface as the temperature is lowered from the diffusion temperature. This occurs because the solid

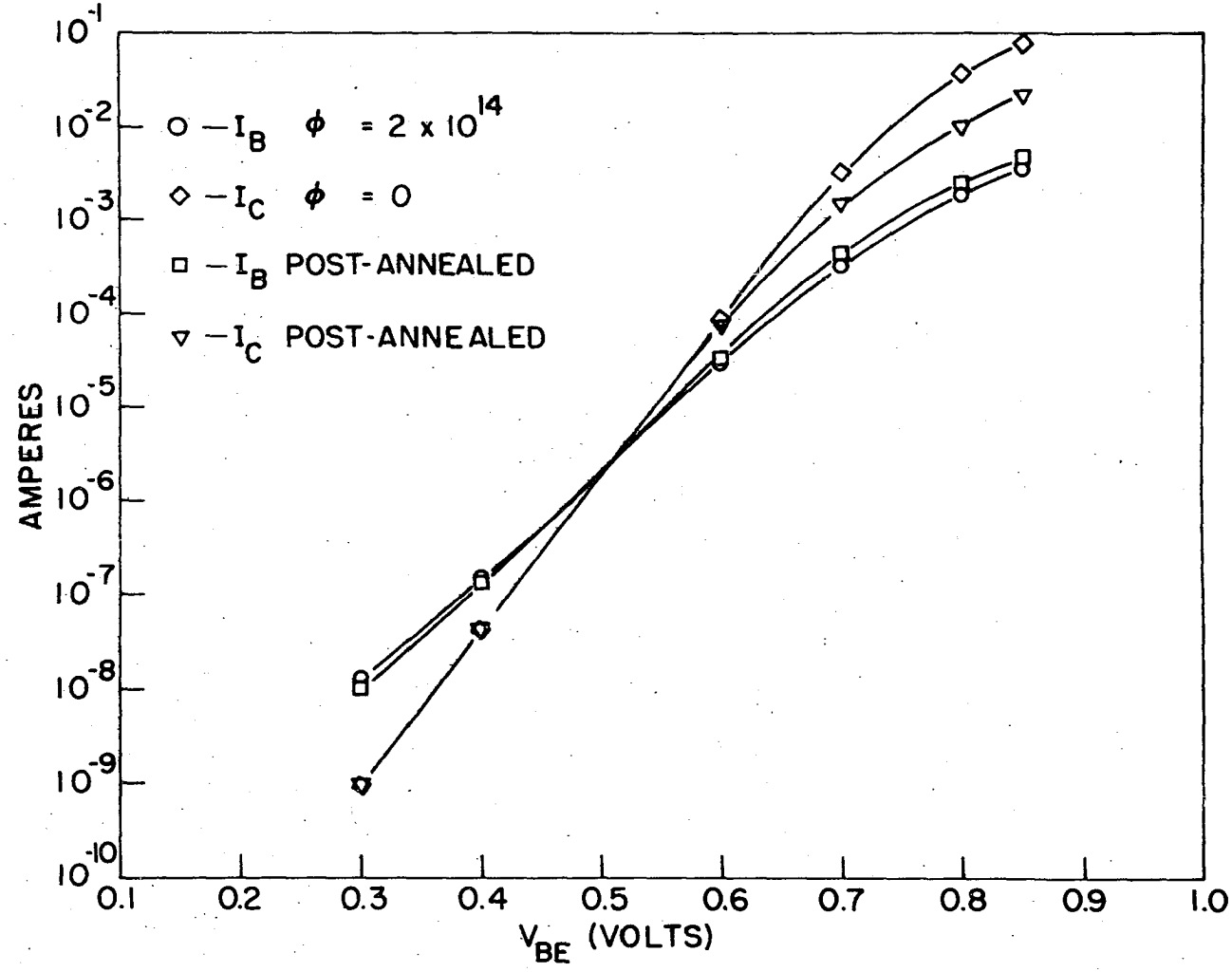

Figure 19. Comparison of I-V characteristics after annealing with I-V characteristics at lower flux levels

solubility of the impurity atoms in the crystal is a function of temperature. It may be possible that these clusters play a dominant role in the determination of the "1.5 component" of current.

Clusters in the bulk regions would be essentially uncharged, since they would be floating in a sea of electrons or a sea of holes, depending upon the conductivity type of the region in which they are located. However, clusters, or microcrystals, in the space-charge region probably would be multiple charged and have energies relatively far away from the band edge. Since the cross-section is related to the charge and the depth from the band edge to the impurity level and increases with increasing charge, it is highly possible that these charged clusters have a very adverse effect on the recombination statistics in the space-charge region. If one assumes that the "1.5 component" of current is caused by these clusters, and asks how to verify it, the answer comes naturally that one should introduce clusters in the bulk space-charge region and see if a bulk "1.5 component" of current arises. Neutrons, because of their heavy mass, cause damage in the form of clusters of atoms. Neutron irradiation is observed to increase the "1.5 component," and it is further observed that this "1.5 component" flows in the bulk region, and therefore must arise in the bulk space charge region. This would tend to verify the conclusion that the "1.5 component" of current depends predominantly on the effects of the clusters of the impurity centers or recombination sites.

1. Electron irradiation

Since the damage sites from neutrons are clusters and since these clusters give rise to a "1.5 component" of current, one may suppose, then, that if one can irradiate devices in such a way as to introduce point defects, this drastic increase in the "1.5 component" of current ought not to be observed. Electron irradiation produces such point defects, and,

therefore, one may verify the hypothesis outlined above by irradiating devices with electrons. A group of devices were irradiated with 2 MeV electrons by the Van de Graaff accelerator at Sandia Laboratory. The results obtained indicate that the electron irradiation up to a level of 10^{16} electrons/cm^2 did not give rise to a "1.5 component" of current, tending to verify the hypothesis that the recombination sites of the origin of the "1.5 component" of current is due to multiple charged clusters in the space-charge region. The devices were further irradiated to a level of 10^{17} electrons/cm^2 but no meaningful interpretation of the data was possible as the characteristics were essentially destroyed by surface effects induced by the ionizing radiation.

IV. DISCUSSION

A. Significance of Present Work

The significance of the present work is that it shows that the base recombination term, which in the past has been held responsible for all the neutron-induced degradation of transistor current gain, is not solely responsible but that the emitter efficiency, which in the past has been assumed to be constant for all values of flux, is indeed a very sharply decreasing function of integrated neutron flux and is responsible for a large fraction of the neutron degradation of transistor current gain. Also significant in this work are the measurements of the mobility, the sheet carrier density, and the resistivity in the base region. It had been thought in the past that the changes in the base region parameters would be similar to changes observed in bulk material. This, however, is the first effort to verify this. The work does, indeed, verify this assumption. Also significant are the indications that the anomalous neutron-induced component of current arises from the same type of recombination centers as the previously identified "surface-perimeter current" (7, 8), and that the neutron-induced recombination centers anneal at different rates in the bulk and space charge regions.

B. Further Work Needed

It should be realized that this investigation covers only the low and intermediate current levels and, therefore, the investigation of the emitter efficiency should be extended to the high-current region where conductivity modulation sets in.

Inspection of the curve of base transport factor versus integrated neutron flux reveals some curvature at low flux levels and this anomaly

in the supposedly linear decrease in the base transport factor at low flux levels should be investigated.

The temperature dependence of the anomalous neutron-induced component of current should be investigated more carefully and over a wider temperature range.

The apparent different annealing rates for the neutron and space charge regions as revealed in the effects on the base and collector currents should be investigated very carefully.

V. BIBLIOGRAPHY

1. The effect of nuclear radiation on semiconductor devices. Battelle Memorial Institute, Radiation Effects Information Center (Columbus, Ohio) REIC Report No. 10. April 30, 1960; and Addendum. July 15, 1961.*

2. Loferski, J. K. Analysis of the effect of nuclear radiation on transistors. J. Appl. Phys. 29: 35-40. 1958.

3. Messenger, G. C. and Spratt, J. P. The effects of neutron irradiation on germanium and silicon. Proc. Inst. Radio Engrs. 46: 1038-1044. 1958.

4. Easley, J. W. and Dooley, J. A. On the neutron bombardment reduction of transistor current gain. J. Appl. Phys. 31: 1024-1028. 1960.

5. Hood, J. A. Predicting the current gain degradation in npn silicon transistors after irradiation by high-energy neutrons. Sandia Laboratory (Albuquerque, N.M.) [Publication] SC-TM-64-69. 1964.

6. Easley, J. W. Radiation damage to semiconductor devices. Sandia Laboratory (Albuquerque, N.M.) [Publication] SCR-532. 1962.

7. Iwersen, J. W., Bray, A. R., and Kleinmack, J. J. Low-current alpha in silicon transistors. Inst. Radio Engrs. Trans. on Electron Devices ED-9: 474-478. 1962.

8. Coppen, P. J. and Matzen, W. T. Distribution of recombination current in emitter-base junctions of silicon transistors. Inst. Radio Engrs. Trans. on Electron Devices ED-9: 75-81. 1962.

9. Shockley, W. The theory of p-n junctions in semiconductors and p-n junction devices. Bell System Tech. J. 28: 435-589. 1949.

10. Moll, J. L. and Ross, I. M. The dependence of transistor parameters on the distribution of base layer resistivity. Proc. Inst. Radio Engrs. 44: 72-78. 1956.

---

*Note: This is a summary of the information available. It references most of the important work done in the field.

11. Sah, C. T., Noyce, R. N., and Shockley, W. Carrier generation and recombination in p-n junctions and p-n junction characteristics. Proc. Inst. Radio Engrs. 45: 1228-1243. 1957.

12. Sah, C. T. Effect of recombination and channel on p-n junction and transistor characteristics. Inst. Radio Engrs. Trans. on Electron Devices ED-9: 94-108. 1962.

13. DeNure, D. G. Effects of fast neutron bombardment on type 2N559 and 2N559E epitaxial pnp germanium switching transistors. Bell Telephone Laboratory (Murray Hill, N. J.) [Publication] MM-61-4252-33. 1961.

14. Hood, J. A. Degradation of npn silicon planar transistors with bombardment by high-energy neutrons. Sandia Laboratory (Albuquerque, N. M) [Publication] SC-TM-261-63(14). 1963.

15. Hood, J. A. Neutron-induced degradation of commercial transistors. Sandia Laboratory (Albuquerque, N.M.) [Publication] SC-TM-129-63(14). 1963.

16. Westmark, C. I. and Rice, W. H. Radiation-induced degradation of dc current gain and collector-to-emitter saturation voltage for selected power transistors. Sandia Laboratory (Albuquerque, N.M.) [Publication] SC-TM-223-63(14). 1963.

17. Sanders, H. H. Neutron permanent damage data for the 2N1675 transistor. Sandia Laboratory (Albuquerque, N. M.) [Publication] SC-RR-65-550. 1964.

18. Manlief, S. K. A method of measuring the minority carrier base transit time in a junction transistor exposed to a neutron environment. Sandia Laboratory (Albuquerque, N.M.) [Publication] SC-TM-314-63(14). 1963.

19. Levy, G. F., Fouse, R. R., and Castner, S. V. The effects of nuclear radiation on some selected semiconductor devices. Proc. of the 2nd Conf. on Nuclear Radiation Effects on Semiconductor Devices, Materials and Circuits: 76-81. 1959.

20. Loferski, J. J. A brief resume of radiation effects on semiconductor materials and devices. Proc. of the 2nd Conf. on Nuclear Radiation Effects on Semiconductor Devices, Materials and Circuits: 8-10. 1959.

21. Smits, F. M. On the energy dependence of neutron damage in silicon transistors. Sandia Laboratory (Albuquerque, N.M.) [Publication] SC-R-64-196. 1964.

22. Sander, H. H. Room temperature annealing of silicon transistor parameters degraded by a burst of neutrons. Sandia Laboratory (Albuquerque, N.M.) [Publication] SC-R-64-192. 1964.

23. Roth, H. and van Lint, Victor A. J. High energy electron irradiation of germanium and silicon. Proc. of the 2nd Conf. on Nuclear Radiation Effects on Semiconductor Devices, Materials and Circuits: 11-13. 1959.

24. Walters, A. E. Minority carrier lifetime in neutron-bombarded germanium. Proc. of the 2nd Conf. on Nuclear Radiation Effects on Semiconductor Devices, Materials and Circuits: 35-38. 1959.

25. Pomeroy, D. Radiation effects on semiconductors. Proc. of the 2nd Conf. on Nuclear Radiation Effects on Semiconductor Devices, Materials and Circuits: 71-75. 1959.

26. Billington, D. S. and Crawford, J. H., Jr. Radiation damage in solids. Princeton, N.J., Princeton University Press. 1961.

27. Wertheim, G. Radiation effects in semiconductors. Nucleonics 20, No. 7: 47-50. 1962.

28. Stein, H. J. Introduction rate of electrically active defects in silicon by nuclear radiation. Sandia Laboratory (Albuquerque, N.M.) [Publication] SC-R-64-193. 1964.

29. Hood, J. A. Predicting the current gain degradation in npn silicon transistors after irradiation by high-energy neutrons. Sandia Laboratory (Albuquerque, N.M.) [Publication] SC-TM-64-69. 1964.

30. Shockley, W. The theory of p-n junctions in semiconductors and p-n junction devices. Bell System Tech. J. 28: 435-589. 1949.

31. Webster, W. M. On the variation of junction-transistor current-amplification factor with emitter current. Proc. Inst. Radio Engrs. 42: 914-920. 1954.

32. Rittner, E. S. Extension of the theory of the junction transistor. Phys. Rev. 94: 1161-1171. 1954.

33. Fletcher, N. H. Note on "the variation of junction transistor current amplification factor with emitter current". Proc. Inst. Radio Engrs. 44: 1475-1476. 1956.

34. Matz, A. W. Variation of junction transistor current amplification factor with emitter current. Proc. Inst. Radio Engrs. 46: 616-617. 1958.

35. Jakits, O. H. Some comments on "Webster's Equation". Inst. Elect. Elec. Engrs. Trans. on Electron Devices ED-10: 292-294. 1963.

36. Tanenbaum, M. and Thomas, D. E. Diffused emitter and base silicon transistors. Bell System Tech. J. 35: 1-22. 1956.

37. Boothroyd, A. R. and Trofimenkoff, F. N. Determination of the physical parameters of transistors of single- and double-diffused structure. Inst. Elect. Elec. Engrs. Trans. on Electron Devices ED-10: 149-163. 1963.

38. Shockley, W. and Read, W. T., Jr. Statistics of the recombinations of holes and electrons. Phys. Rev. 87: 835-842. 1952.

39. Shockley, W. Electrons, holes, and traps. Proc. Inst. Radio Engrs. 46: 973-990. 1958.

40. Pearson, G. L. and Bardeen, J. Electrical properties of pure silicon, and silicon alloys containing boron and phosphorus. Phys. Rev. 75: 865-883. 1949.

41. Volger, J. Note on the Hall potential across an inhomogeneous conductor. Phys. Rev. 79: 1023-1024. 1950.

42. Debye, P. P. and Conwell, E. M. Electrical properties of n-type germanium. Phys. Rev. 93: 693-706. 1954.

43. Valdes, L. B. Resistivity measurements on germanium for transistors. Proc. Inst. Radio Engrs. 43: 420-427. 1954.

44. Flanagan, W. F., Flinn, P. H., and Averbach, B. L. Shorting and field corrections in Hall measurements. Rev. Sci. Insts. 25: 593-595. 1954.

45. Wick, R. F. Solution of the field problem of the germanium gyrator. J. Appl. Phys. 25: 741-756. 1954.

46. Fritzsche, H. and Lark-Horowitz, K. Electrical properties of p-type indium antimonide at low temperatures. Phys. Rev. 99: 400-405. 1955.

47. Tauc, J. Electronic phenomena in semiconductors with a temperature gradient. (Translated edition) Czechosl. J. Phys. 6, No. 2: 108-123. 1956.

48. Prabble, J. R. and Wolfe, R. Geometrical effects in transverse magnetoresistance measurements. J. Elect. Control 3: 259-266. 1957.

49. van der Pauw, L. J. A method of measuring specific resistivity and Hall effect of discs of arbitrary shape. Phillips Research Reports 13, No. 1: 1-9. 1958.

50. van der Pauw, L. J. A method of measuring the resistivity and Hall coefficient on lamellae of arbitrary shape. Phillips Technical Review 20, No. 8: 220-224. 1958/59.

51. Broudy, R. M. Galvanomagnetic coefficients of arbitrary geometry. J. Appl. Phys. 29: 853-855. 1958.

52. Hannay, N. B. Semiconductors. New York, N.Y., Reinhold Pub. Co. 1959.

53. Putley, E. H. The Hall effect and related phenomena. London, U. K., Butterworths. 1960.

54. Hall, R. N. An analysis of the performance of thermoelectric devices made from long-lifetime semiconductors. Solid State Electronics 2: 115-122. 1961.

55. Lange, J. Method for Hall mobility and resistivity measurements on thin layers. Bell Telephone Laboratory (Murray Hill, N.J.) [Publication] MM-63-2821-1. 1963.

56. Mason, D. R. Semiconductor theory and technology. Ann Arbor, Mich., University of Michigan Press. 1963.

57. Barrer, R. M. Diffusion in and through solids. New York, N.Y., Macmillan. 1941.

58. Looney, D. H. Fourteenth interim technical report for period 1 October 1954 to 31 December 1954. U. S. Army Signal Corp. [Publication] DA 36039-sc-5589. 1955.

59. Stein, H. J. Introduction rate of electrically active defects in silicon by nuclear radiation. Sandia Laboratory (Albuquerque, N.M.) [Publication] SC-R-64-193. 1964.

60. Wertheim, G. K. Neutron bombardment damage in silicon. Phys. Rev. 111: 1500-1505. 1958.

61. Hunter, L. P. Handbook of semiconductor electronics. 2nd ed. New York, N.Y., McGraw-Hill Book Co., Inc. 1962.

62. O'Brien, P. D. Hazards evaluation of the Sandia Pulsed Reactor Facility (SPRF). Sandia Laboratory (Albuquerque, N.M.) [Publication] SC-4357A(RR). 1961.

63. Buckalew, W. H. Neutron flux and spectrum measurements in the Sandia Pulsed Reactor Facility (SPRF). Sandia Laboratory (Albuquerque, N.M.) [Publication] SCR-463. 1962.

VI. ACKNOWLEDGEMENTS

The author is happy to acknowledge the efforts of Professors R. G. Brown and A. V. Pohm of Iowa State University and the efforts of Dr. F. M. Smits and A. W. Snyder of Sandia Laboratory in directing this research effort.

A special note of thanks goes to Mr. C. R. Jenkins for his valuable assistance in the fabrication and operation of test equipment.

I wish to express my appreciation to my co-workers and colleagues at Sandia Laboratory and Iowa State University for many useful and interesting discussions.

Appreciation is expressed to the Atomic Energy Commission and to Sandia Laboratory for supporting this research effort.

Miss L. D. Patterson, Mrs. Dorothy Mann and their able assistants have my heartfelt gratitude for their work in the preparation of this manuscript.

VII. APPENDIX - EXPERIMENTAL APPARATUS

A. Test Circuits and Test Equipments

1. Sample holder circuitry

The sample holder circuitry, illustrated in Figure 20, was used for the measurement of the current-voltage characteristics of both single-base and double-base transistors. The circuit, as used for the single-base transistor, essentially provides for an emitter-to-base bias with the base and collector leads shorted together through the current sampler (described below). For use with double-base transistors, the circuit provides for the application of a base 1-to-base 2 bias.

The sample holder consists of a floating, guarded, and shielded circuitry mounted inside a temperature control oven (See Figure 20). The test device socket and a part of the associated test circuitry are located within these shields. This circuitry was placed inside the oven so that the interconnecting leads would be as short as possible. All leads from the device socket were fitted with ferrite beads to suppress oscillation. The device socket itself is a 4-terminal type and will accept either single-base or double-base transistors. The selection of single-base or double-base transistors depends upon switch SW1. Provision was made to apply a base 1-to-base 2 bias in the 4-terminal configuration. Switch SW2 determines whether base 1 is positive, base 2 is positive,, or whether base 1 and base 2 are shorted together. Potentiometer R1 adjusts the bias level. Base 1-to-base 2 bias and current may be measured by the use of output connectors J2 and J3. Connector J2 is used to measure the current and J3 the bias. For normal-transistor operation J2 must be shorted as it is part of the current path. The base, emitter, collector, remote voltage sensing, and

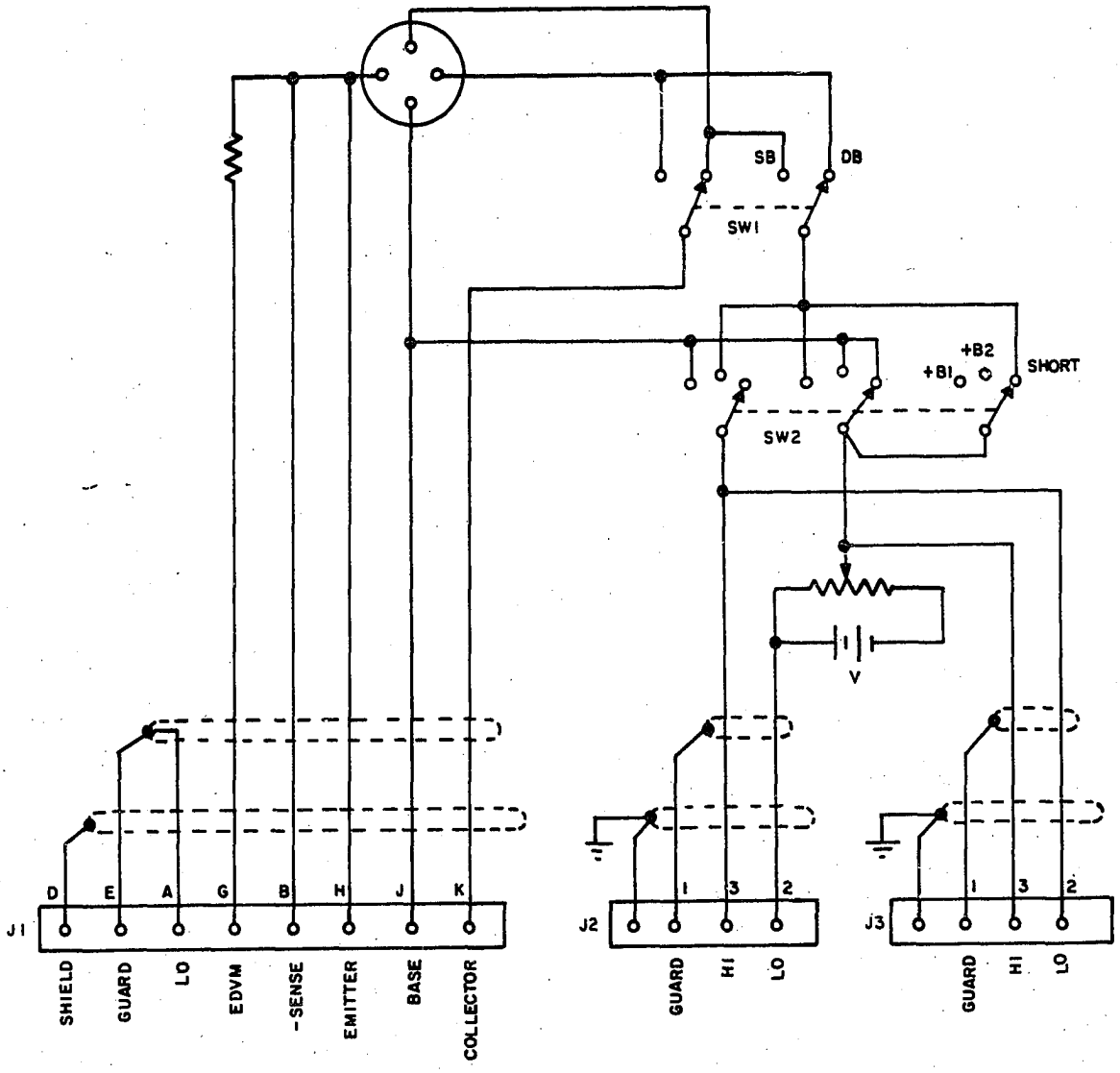

Figure 20. Sample holder circuitry

base-emitter digital voltmeter leads are all brought out in a single guarded, grounded cable. The chassis in which the components are mounted forms the guard shield and the oven forms the grounded shield.

2. Current sampler

The current sampler (Figures 21, 22, 23) provides a means of selecting the proper current sampling resistor, switching between the base and collector circuits, and also provides a 10-line code for resistor identification. These operations are accomplished by means of remote programming from Dymec 2901A/2902A scanners. The appropriate resistor is selected remotely in advance by programming a contact closure in the Dymec 2901A/2902A scanners. Another contact closure selects either base current sampling or collector current sampling. These are respectively relays K-9 and K-10. Relays K-1 through K-8 select the sampling resistors. These resistors range in value from 500,000 ohms to 0.025 ohm.

Relays K-1 through K-8 draw a high current. To avoid exceeding the current capability of the diode programming pins in the Dymec 2901A/2902A scanners, relays KD-1 through KD-8 are used to drive K-1 through K-8 and to provide a 10-line code for resistor identification.

To prevent the possibility of an open base or collector circuit which might damage the device being measured, or the test equipment itself, the wiring is such that if no other resistor is programmed, resistor R-1, whose value is 0.025 ohm, is in the current sampling circuit. Each time a resistor other than R-1 is programmed, relay K-1 is also pulled to remove R-1 from the circuit. The identification code for R-1, controlled by relay KD-1, is not activated unless R-1 is actually programmed in the scanner. All resistors and their relay contacts are mounted inside the guard shield and the resistor relay coils are mounted

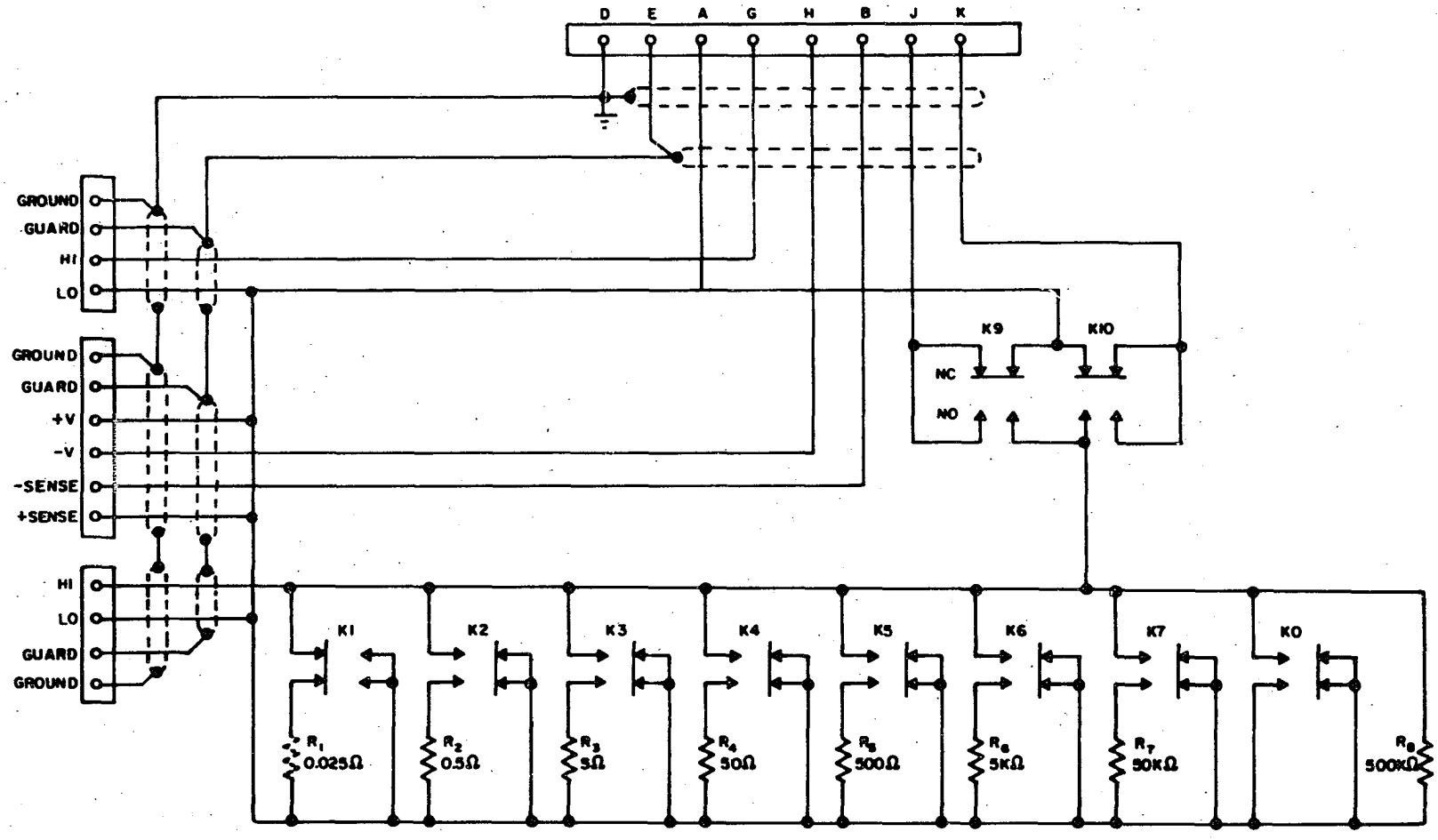

Figure 21. Current sampler - precision resistor and switching circuitry

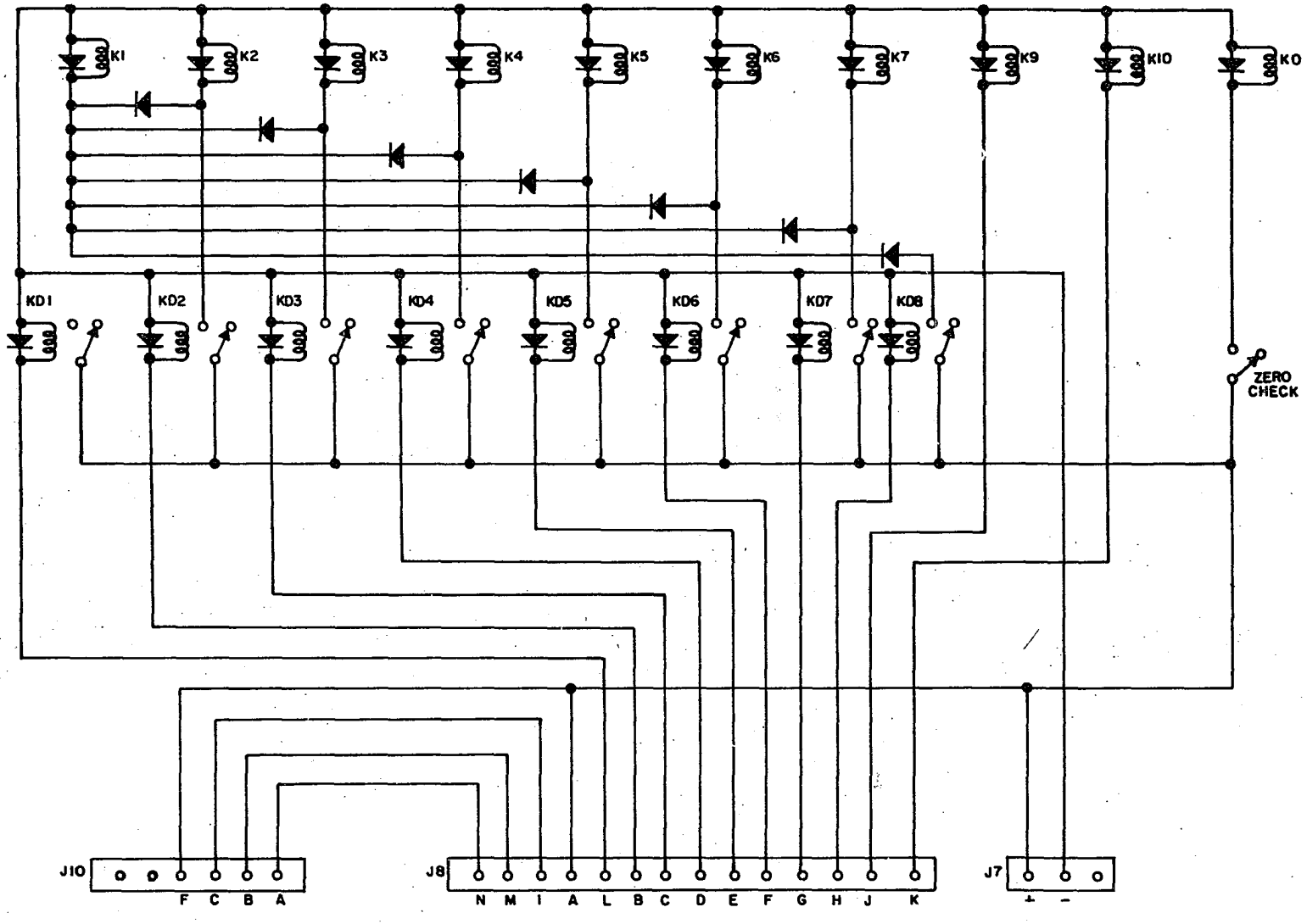

Figure 22. Current sampler - control circuitry

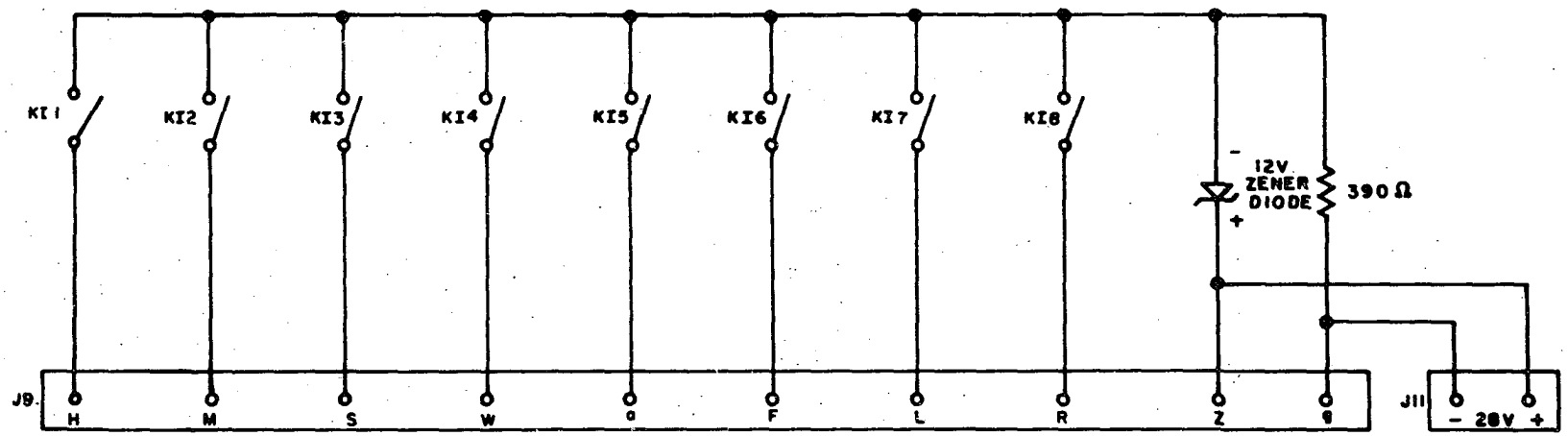

Figure 23. Current sampler - 10-line decimal code identification output

between the guard shield and the ground shield. The relays which control the resistor relays and provide the 10-line code are outside the ground shield. This type of mounting reduces the possibility of noise pickup from the coils. The program input jack is J8. The 10-line output jack is J9. The contact closures from the Dymec 2901A/2902A scanners to the automatic driver/programmer are routed through J10.

3. Hall effect and sheet resistivity circuitry

The circuitry illustrated in Figure 24 allows the measurement of the Hall-effect voltage and sheet resistivity in the base region under the emitter. The double-base transistor has its two base leads inserted in J2. With the ganged switch S3 in the position illustrated, switch S2 allows a reversal of the current flowing from base 1 to base 2 and a sampling of the current by measuring the potential across the 100 ohm precision resistor.

The Hall-effect device is a five terminal device which is inserted in J1 for the measurement of the Hall effect. As switch S3 is stepped the eight measurements needed for the determination of the Hall constant and the sheet resistivity (40 - 56) of the base region of the Hall effect transistors are made and in addition a zero check is made on the digital voltmeter and the current is sampled.

A John Fluke 383B voltage/current calibrator (a 0.025% instrument) was used as the current source and the digital voltmeter was a Dymec model 2401A (a 0.01% instrument). The output of the voltmeter was recorded on a Hewlett Packard H25-562AR digital recorder. The digital recorder output was reduced to magnetic tape and the data subsequently were reduced by means of a computer program written for the CDC 1604 computer. The computer output, in tabular form, consists of the sheet resistivity, Hall constant, sheet carrier concentration, the Hall mobility, and normalized values of the above.

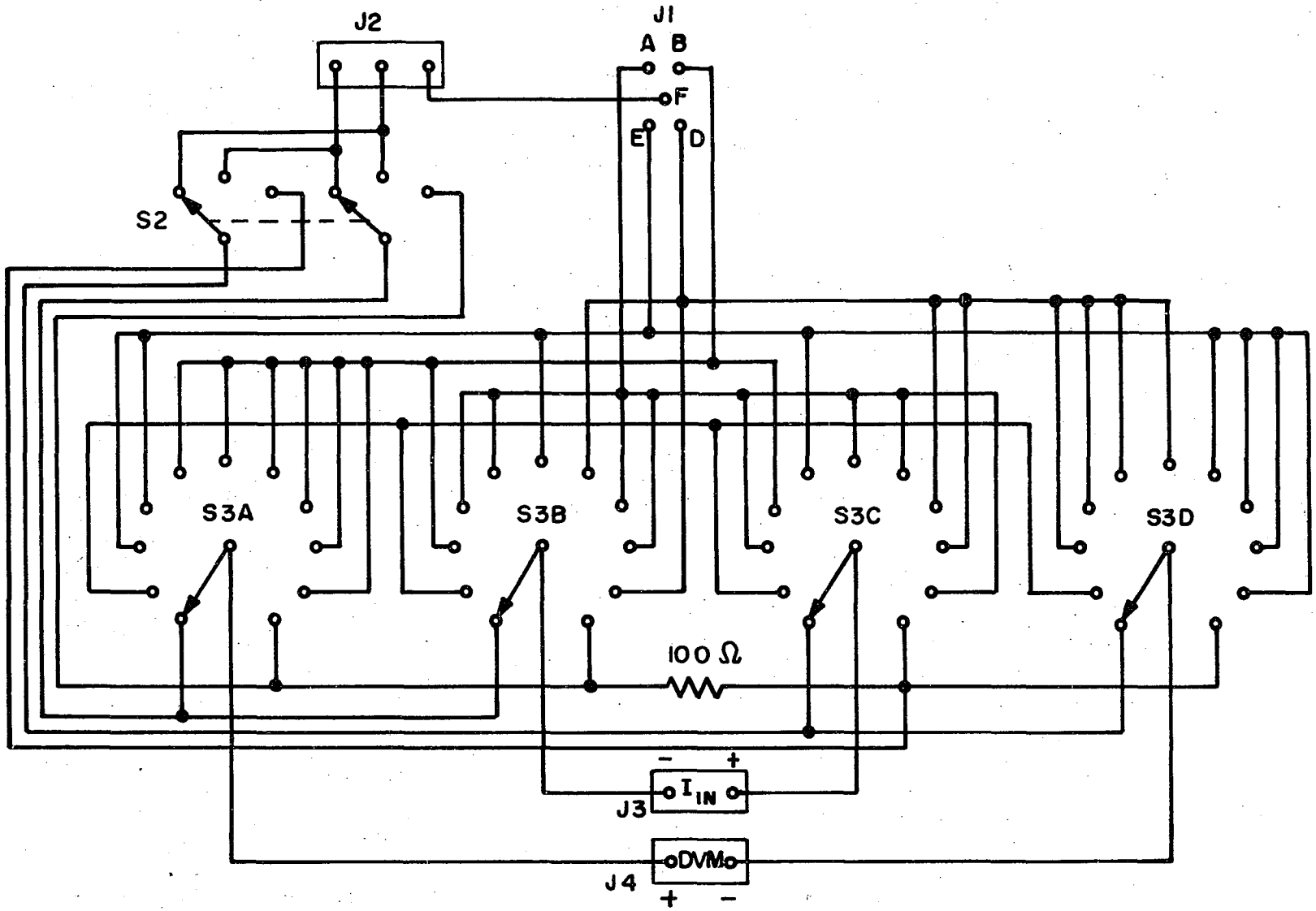

Figure 24. Hall effect and sheet resistance measurement circuitry

A block diagram of the measuring equipment described above is illustrated in Figure 25.

4. John Fluke 383B voltage/current calibrator

The John Fluke Model 383B voltage/current calibrator is a 0.025 percent instrument. It has one voltage range of 0 to 50 volts and four current ranges of 0 to 5 milliamps, 0 to 50 milliamps, 0 to 500 milliamps, and 0 to 2 amperes. It may be programmed from 0.1 millivolt to 50 volts in 0.1 millivolt steps and from 0.01 microampere to 2 amperes in variable steps ranging from 0.01 μa on the lowest range to 10 μa on the highest range. Programming is accomplished by means of a remote binary coded decimal programming input.

Binary coded decimal inputs are provided from an automatic driver/programmer (described below) for the function and ranges in addition to the six digits provided for the magnitude of the DC current or voltage output. The ripple on the DC output is less than 50 microvolts rms.

5. Automatic driver/programmer

An automatic driver/programmer was designed and fabricated to provide a programmable binary coded decimal output to drive the John Fluke 383B voltage/current calibrator described above. The driver/programmer produces an output of four decimal digits each composed of four binary digits in a 4421 code plus three binary digits for range and function. Logical "1" is -28 ±4 volts and logical "0" is 0 volts. The driver/programmer is used to program the John Fluke 383B in a constant voltage or a constant current mode. In the constant voltage mode the driver/programmer will program the John Fluke 383B from 10 millivolts to 50 volts in 10 millivolt increments and, in the constant current mode, from 1 microamp to 2 amperes in variable increments beginning

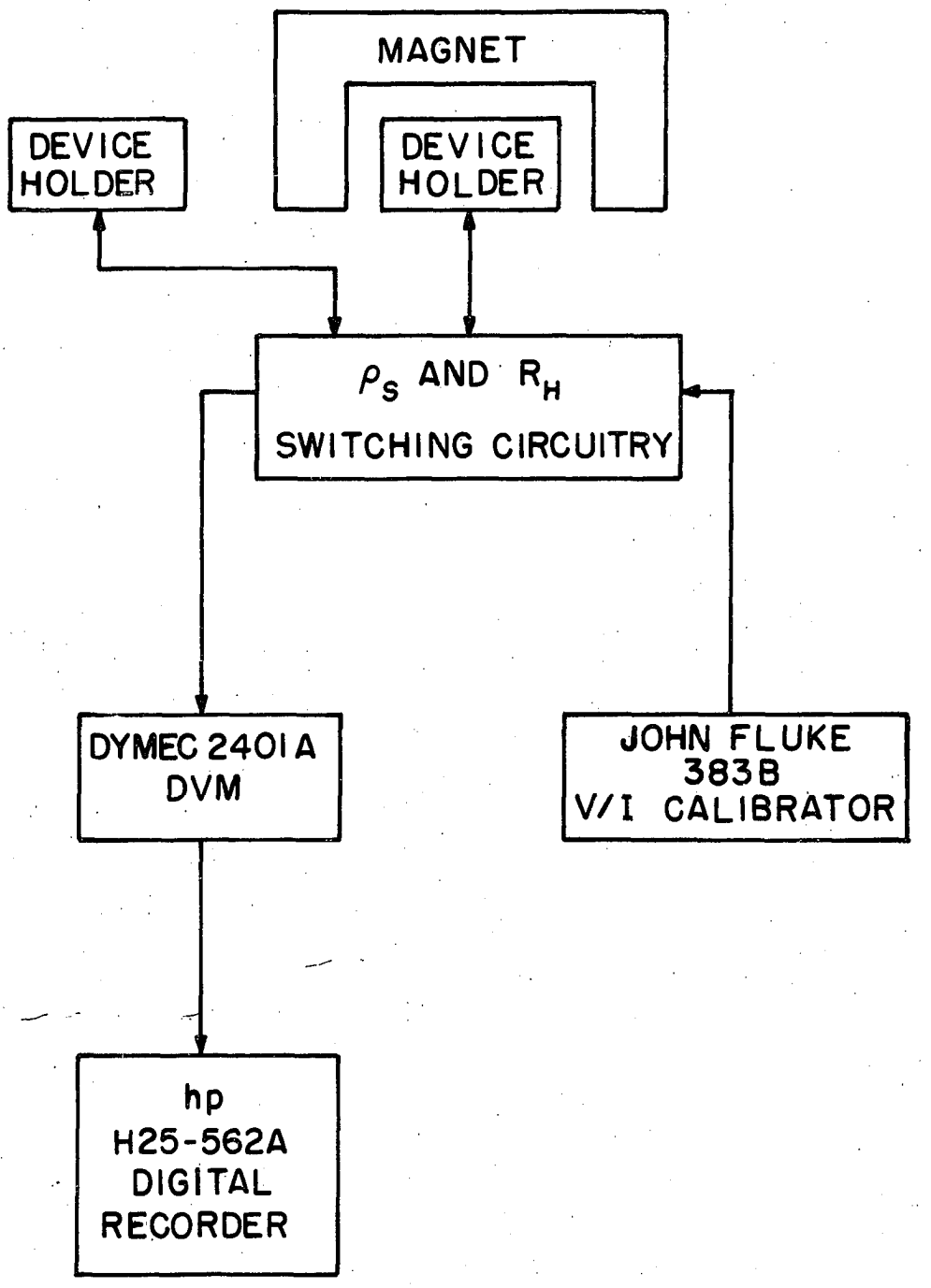

Figure 25. Block diagram of R_H and ρ_s measuring equipments

on the lowest range with 1 microampere and progressing to 1 milliampere increments on the 2 ampere range.

The binary coded decimal output is generated by a 100 by 26 position diode pin matrix board as illustrated in Figure 26. The diodes used are mounted in small pin plugs so that they may be readily inserted or removed to change the programming. A binary "1" is generated by inserting a diode pin in the appropriate jack in the matrix board. A binary "0" is the absence of such a diode pin. The 100-positions of the matrix are connected to five levels of a 20-position 8-level rotary stepping switch. This is switch SW10 in Figure 27. Switch SW10 and switch SW12, a 10-position, 3-level stepping switch, are used together to step through the 100 channels in sequence. The configuration of switch SW10 is such that when one set of wipers steps from the 20th position a parallel set of wipers steps to the first position making the switch continuous. Switch SW12 has 5 positions of its first level wired to the wipers of the five levels of switch SW10. The input voltage to generate the binary coded decimal code is brought into the wiper of switch SW12. Therefore, only one level at a time of switch SW10 will have a voltage applied. The coil of switch SW12 is wired such that every time switch SW10 steps from its 20th position to the first position, switch SW12 steps one position, making the next level active. The combination of switch SW10 and switch SW12 appears, then, as a single 100-position, single-level rotary switch. The drive circuit for the driver/programmer is shown in Figure 28. K10 is the coil of switch SW10. K11 is the coil of mercury relay switch SW11, and K12S and K12R are step and reset coils of switch SW12. Q1 is the transistor switch to drive the mercury relay K10. A contact closure in the Dymec 2901A scanner/programmer is applied across contacts B and F of J17, shorting one side of capacitor C1 to common. C1 discharges through R2, producing a negative voltage

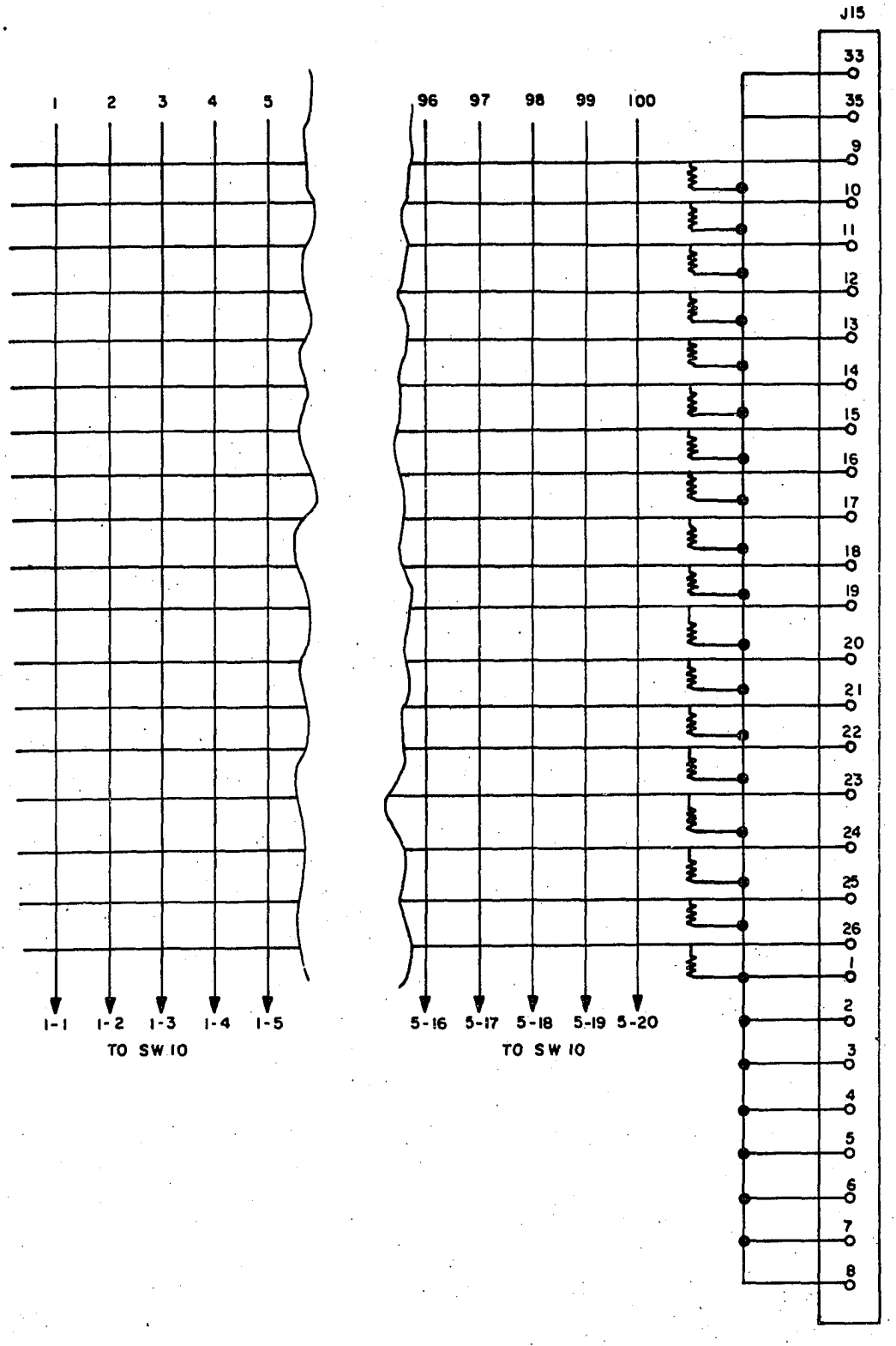

Figure 26. Automatic driver/programmer - programs boards

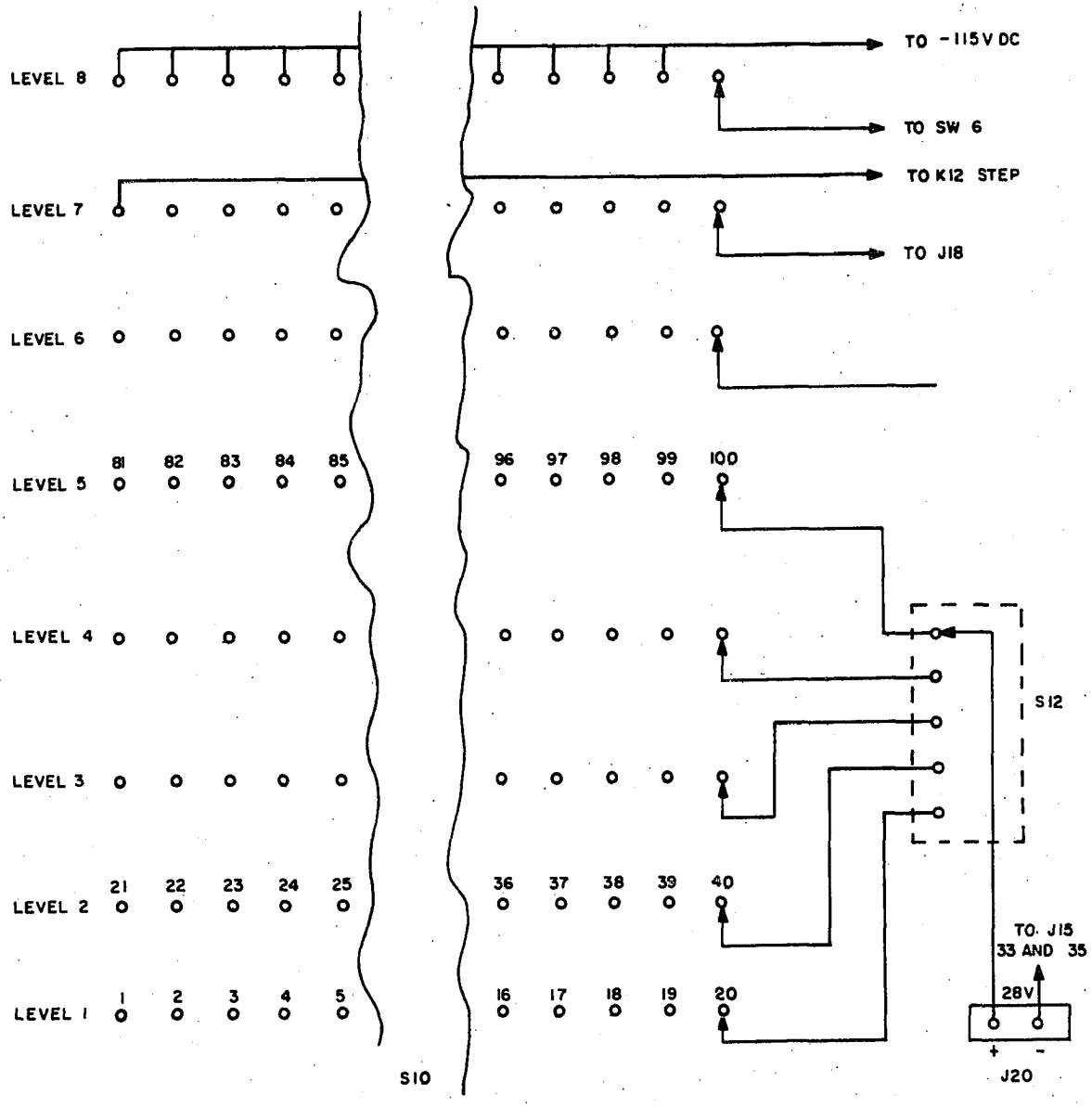

Figure 27. Automatic driver/programmer - stepping switch circuitry

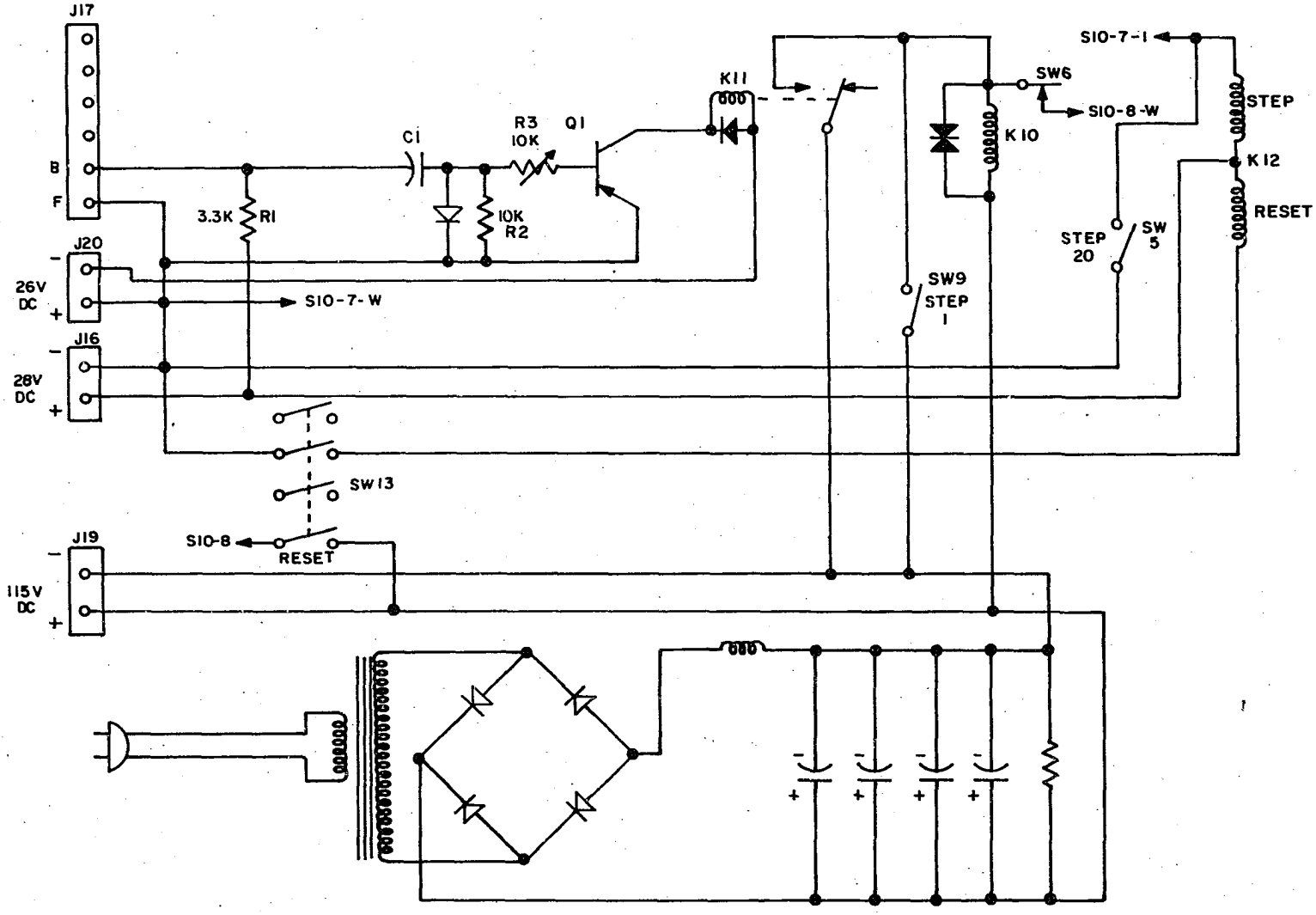

Figure 28. Automatic driver/programmer - control circuitry

which turns on Q1 and closes the contacts on K11 for the length of the discharge time. Contacts K11 apply 110 DC volts to the K10 coil. K10 does not step, however, until the voltage is removed from the coil. When the Dymec 2901A scanner advances to its next channel, the contact closure across B and F of J17 is momentarily broken and C1 charges through diode D1 and resistor R1. R3 is used as the current-limiting resistor and varies the time Q1 is in saturation. Provision is made to manually advance the driver/programmer either 1 or 20 positions at a time. Front panel switch SW9 advances one position and SW5 on the front panel advances 20 positions at a time. Switch SW13 is the reset switch. When switch SW13 is depressed, the voltage is applied to the reset coil of K12 and to the 8th level of switch SW10 (Figure 27) except for one position. The wiper of switch SW10 is connected to switch SW6 which is mechanically linked to K10 (Figure 28). K10 will continuously step until the unwired position of the 8th level is reached. This is the reset position. The 7th level of switch SW10 is used to advance switch SW12 on every 20th step of switch SW10.

6. Manual driver/programmer

In conjunction with the 383B voltage/current calibrator described previously, an additional driver/programmer was fabricated. This one is manually operated by means of thumb switches. It was fabricated to permit use of the 383B to calibrate other equipments. The circuit diagram of this manual driver/programmer is shown in Figure 29.

7. Delta Design oven and CSP solid state controller

The Delta Design oven uses carbon dioxide gas as a coolant and resistance heating as a heat source. The inside dimensions of the oven are 8 x 8 x 10 inches and it is in this space that the sample holder is mounted. The Delta Design CSP solid state temperature controller is

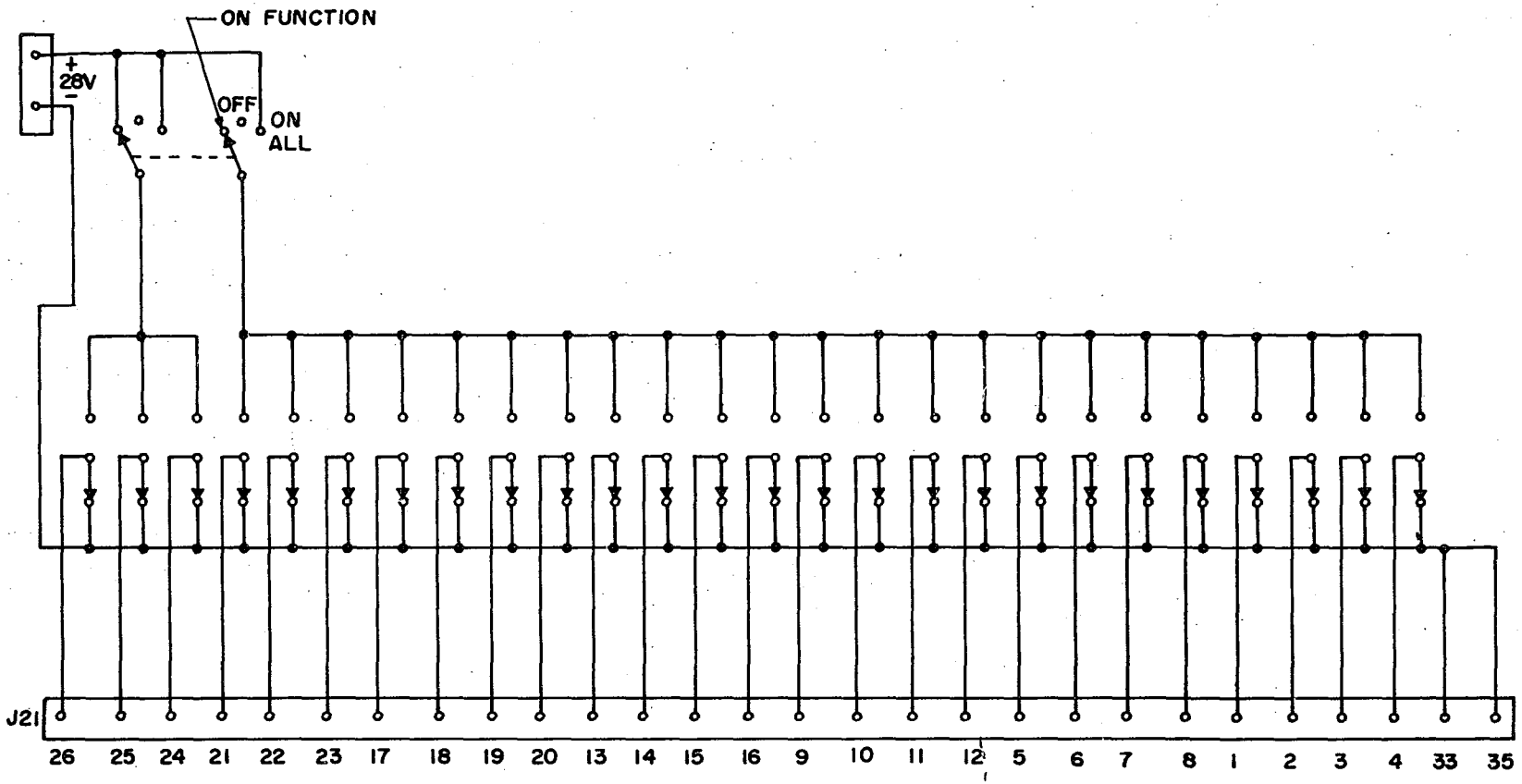

Figure 29. Manual driver/programmer - circuitry

specified to hold the oven to within ±1°F of the setting. The limits on the oven are -100°F (-73.3°C) and +600°F (+315.6°C).

8. Sanborn model 4300 amplifiers

The Sanborn model 4300 amplifiers were modified at the factory according to specifications. The specifications, which these amplifiers were modified to meet, are a one megohm resistive impedance input and noise level of less than 10 microvolts referred to the input.

9. Non-Linear Systems model M24 digital voltmeter

The Non-Linear Systems model M24 digital voltmeters were modified slightly. This modification consisted of installing much higher gain transistors in the circuits for the 10-line output codes so as to speed up the response or the rise time of the output signal to match the speed of the Gulton system and the paralleling of the indicator lamps with a 10K resistor so that an output would still be available in the event that one of the front panel display indicator lamps burned out.

10. Serializer, decoder, recorder and keyboard

The operation of the decoder is to accept the voltage signals from each of the two digital voltmeters. When both signals are received, the decoder translates or decodes the ten-line code received from the NLS digital voltmeters into four-line codes. This information is then transferred to the serializer where it is serialized. The serializing consists of placing in sequence an arrow, the ID digit from the current sampler, the two identification digits from the Dymec 2901A/2902A scanners, and the two 7-digit voltmeter readings. The 7-digit voltmeter readings each consist of the polarity, four voltmeter digits, the sign of the exponent, and the exponent. When the information is serialized, a signal is generated to transfer the information to the Precision Instruments tape recorder. The model RSL150-7C incremental tape recorder has a stepping

rate of 100 steps per second and a packing density of 200 bits per inch. The information is recorded on the magnetic tape by the tape recorder sequentially. That is to say, for a hundred-data word record there will be 1800 characters in sequence. Since this record is much too long to be of usable size for the Control Data Corporation (CDC) 1604 computer, it is first passed through the CDC 160A computer where it is broken up into 80 character records which are then transferred to a different magnetic tape and transmitted to the 1604 computer for data reduction purposes. The Invac keyboard used with this system allows the typing of lead or heading information for each data run at the beginning of said data run.

The binary codes and the alpha-numeric characters which the Invac keyboard is capable of outputting to the magnetic tape unit are shown in Figure 30.

11. Input scanner programmers

The Dymec model DY-2901A input scanner/programmer and the DY-2902A slave scanners provide automatic scanning of 25 signal inputs each and up to 100 channels with a master and three slave units. The channels are selected by means of pushbuttons and accurate transference of microvolt signals is made with shielded pair leads and gold-plated connectors. The scanners have a flexible system control with diode pin matrix board programming of external functions and internal measurement delay. In addition, channel identification outputs are available for use by the auxiliary equipments. The model DY-2901A input scanner/programmer is designed to transfer, sequentially, information from external signal sources, such as thermocouples, transistors, strain gauges, etc., to one set of measuring and recording equipment. Data points may be scanned continuously or upon local or remote command. To accommodate inputs of different types or levels the DY-2901A

BCD Code

Symbol	Octal	Track							Symbol	Octal	Track						
		C	B	A	8	4	2	1			C	B	A	8	4	2	1
1	01	1	0	0	0	0	0	1	P	47	0	1	0	0	1	1	1
2	02	1	0	0	0	0	1	0	Q	50	0	1	0	1	0	0	0
3	03	0	0	0	0	0	1	1	R	51	1	1	0	1	0	0	1
4	04	1	0	0	0	1	0	0	S	22	0	0	1	0	0	1	0
5	05	0	0	0	0	1	0	1	T	23	1	0	1	0	0	1	1
6	06	0	0	0	0	1	1	0	U	24	0	0	1	0	1	0	0
7	07	1	0	0	0	1	1	1	V	25	1	0	1	0	1	0	1
8	10	1	0	0	1	0	0	0	W	26	1	0	1	0	1	1	0
9	11	0	0	0	1	0	0	1	X	27	0	0	1	0	1	1	1
0	12	0	0	0	1	0	1	0	Y	30	0	0	1	1	0	0	0
A	61	1	1	1	0	0	0	1	Z	31	1	0	1	1	0	0	1
B	62	1	1	1	0	0	1	0	/	21	0	0	1	0	0	0	1
C	63	0	1	1	0	0	1	1	+	60	0	1	1	0	0	0	0
D	64	1	1	1	0	1	0	0	-	40	1	1	0	0	0	0	0
E	65	0	1	1	0	1	0	1	.	73	1	1	1	1	0	1	1
F	66	0	1	1	0	1	1	0	,	33	0	0	1	1	0	1	1
G	67	1	1	1	0	1	1	1	*	54	1	1	0	1	1	0	0
H	70	1	1	1	1	0	0	0	$	53	0	1	0	1	0	1	1
I	71	0	1	1	1	0	0	1	(	34	1	0	1	1	1	0	0
J	41	0	1	0	0	0	0	1	)	74	0	1	1	1	1	0	0
K	42	0	1	0	0	0	1	0	(SPACE)	20	1	0	1	0	0	0	0
L	43	1	1	0	0	0	1	1	→	35	0	0	1	1	1	0	1
M	44	0	1	0	0	1	0	0	=	13	1	0	0	1	0	1	1
N	45	1	1	0	0	1	0	1	GAP		(end of record gap)						
Ø	46	1	1	0	0	1	1	0	EOF		(end of file mark)						

Figure 30. Binary codes and alphanumeric characters output by Invac keyboard

scanner will program the appropriate system operating functions and ranges for each channel by means of diode pin matrix board programming. Channels are pre-selected for measurement merely by depressing the appropriate pushbutton. When the scanner steps to a new channel, it issues a read command to the associated measuring instruments. To allow for stabilization and settling times that may be required by DC amplifiers and AC measuring devices the DY-2901A contains a measurement delay circuit that can be internally programmed to insert a fixed delay in each channel position before the read command is issued. Any one of four delays ranging from 25 to 910 milliseconds may be programmed individually for each channel. The delay of 910 milliseconds was chosen for the work reported here. The delay circuit, of course, is operative in all modes of operation. In addition to the visual display, the DY-2901A provides a 2-digit channel identification output for recording purposes. The model DY-2901A input scanner/programmer has the ability to program, for each input channel, the appropriate functions and ranges for the other units of the system. Programming of up to 15 functions per input channel is accomplished by inserting diode pins in a 25 x 15 point diode pin matrix board. In our application, a second diode pin matrix board was added, allowing a maximum programming of 30 functions per channel. The 2902A slave units are similar to the DY-2901A master unit but omit the power supply, operating mode switches, channel indication, and output switching circuitry, since these features are provided by the DY-2901A and are not necessary for the slave units. The slave units contain both the normal program diode pin matrix board and the auxiliary program diode pin matrix board needed for this work.

B. Irradiation Facilities and Dosimetry

The Sandia Pulsed Reactor Facility (SPRF) (62) was used for the neutron irradiations. The Sandia Pulsed Reactor (SPR) is an unreflected, enriched uranium assembly similar to the Los Alamos Scientific Laboratory's Godiva II. The devices were mounted on a polystyrene block and irradiated at room temperature.

All electron irradiations were performed on the Sandia Laboratory Van de Graaff accelerator. The accelerator is a 2,000,000-volt machine. Samples were mounted in a copper block inside a vacuum chamber at the head of the machine. The impinging electrons pass through a 3-millimeter sheet of aluminum before damaging the devices. The copper block was cooled by boiling nitrogen from a dewar. The vacuum was pulled on the system with a vac-sorb pump.

Sulfur pellets (aluminum clad) and nickel foils were used to determine the total neutron flux for each exposure. A numerical constant was used to obtain integrated flux above 0.01 MeV from the measurements on sulfur and nickel (63).

Dosimetric measurements for the neutron irradiations were performed in the Sandia Corporation dosimetry laboratories. Dosimetric measurements for the electron irradiations were performed by means of a Faraday cup. Accuracy of the dosimetric measurements is estimated to be plus or minus ten percent.

All irradiations were made simultaneously on the transistors and other test structures to insure equal exposure. Testing, except for those temperature runs which are clearly indicated, was performed at a closely regulated 27°C.